



1N7L11M
1N-37-CR
OCIT.
185968
P-72

Annual Report:

DESIGN AND APPLICATION OF ELECTROMECHANICAL ACTUATORS FOR DEEP SPACE MISSIONS

Submitted to:

NASA
Marshall Space Flight Center EP64

Prepared by:

Dr. Tim A. Haskew Dr. John Wander
Assistant Professor Assistant Professor
Department of Electrical Engineering Department of Mechanical Engineering

College of Engineering
The University of Alabama
Box 870286
Tuscaloosa, AL 35487-0286

Reporting Period:
8/16/92 - 8/15/93

BER Report No. 597-163

September 1993

(NASA-CR-194145) DESIGN AND
APPLICATION OF ELECTROMECHANICAL
ACTUATORS FOR DEEP SPACE MISSIONS
Annual Report, 16 Aug. 1992 - 15
Aug. 1993 (Alabama Univ.) 72 p

N94-14134

Unclass

G3/37 0185968

The University of Alabama
College of Engineering
Bureau of Engineering Research
Box 870201
Tuscaloosa, Alabama 35487-0201
Telephone: (205) 348-1591

Annual Report:

**DESIGN AND APPLICATION OF ELECTROMECHANICAL
ACTUATORS FOR DEEP SPACE MISSIONS**

Submitted to:

NASA
Marshall Space Flight Center EP64
ATTN: Rusty Cowan

Prepared by:

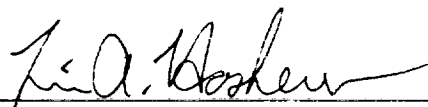
Dr. Tim A. Haskew
Assistant Professor
Department of Electrical Engineering

Dr. John Wander
Assistant Professor
Department of Mechanical Engineering

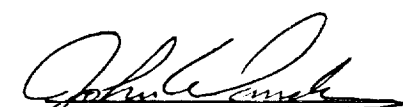
College of Engineering
The University of Alabama
Box 870286
Tuscaloosa, AL 35487-0286

Reporting Period:

8/16/92 - 8/15/93



Tim A. Haskew
Project Director, Co-Principal Investigator



John Wander
Co-Principal Investigator

TABLE OF CONTENTS

I.	Executive Summary	
II.	Phase 1 Task I.1: EMA Modeling and Test Stand Development	
II.1.	Development of EMA Test Facility.....	II.1
II.2.	Preliminary Experiment Schedule for SSME EMAs.....	II.2
II.3.	Analysis for Design of Stiff-Arm SSME Tests.....	II.4
II.4.	Development of SSME TVC with an EMA Similar to Previous Control with a Hydraulic Actuator	II.7
II.5.	References	II.14
III.	Health Monitoring and Fault Diagnosis	
III.1.	Fundamental Philosophy	III.1
III.2.	The Kalman Filter	III.2
III.2.1.	The Separately Excited DC Machine	III.5
III.2.2.	Application of the Kalman Filter	III.8
III.3.	Use of the Kalman Filter for Health Monitoring And Fault Diagnosis	III.8
III.3.1.	Linearized and Extended Kalman Filters	III.11
III.3.2.	Adaptive Kalman Filtering	III.15
III.4.	Continuing Efforts	III.23
III.5.	Hardware Implementation	III.25
III.6.	References.....	III.25
	APPENDIX A: Test Stand Construction Proposal	
	APPENDIX B: Detailed Test Stand Drawings	

I. EXECUTIVE SUMMARY

This document constitutes the first annual report submitted on NASA grant NAG8-240, "Design and Application of Electromechanical Actuators for Deep Space Missions." The reporting period for this report is 8/16/92 through 8/15/93. However, the primary focus of this document will be work performed since submission of our semi-annual progress report in February 1993.

During the first year of this three-year continuing grant, a total of two faculty members and six graduate students have been actively involved in research efforts. As a result of such involvement, substantial progress has been made. We currently feel confident in providing guidelines for motor and control strategy selection in electromechanical actuators to be used in thrust vector control (TVC) applications.

A small portion of this work was presented in the semi-annual report. At this point, we have implemented highly detailed simulations of various motor/drive systems. The primary motor candidates were the brushless dc machine, permanent magnet synchronous machine, and the induction machine. The primary control implementations were pulse width modulation and hysteresis current control. Each of the two control strategies have been applied to each of the three motor choices. With either pulse width modulation or hysteresis current control, the induction machine was always vector controlled. We have defined a standard test position command sequence for system performance evaluation. Currently, we are gathering all of the necessary data for formal presentation of the results. Briefly stated for TVC application, we feel that the brushless dc machine operating under PWM current control is the best option. Substantial details on the topic, with supporting simulation results, will be provided later, in the form of a technical paper prepared for submission and also in the next progress report with more detail than allowed for paper publication.

Additionally, we have completed the design of a versatile and flexible test facility for roller screws and complete TVC actuators. This facility is to be housed in the Electrical Engineering Power/Machines Laboratory located in the East Engineering Building on The University of Alabama Campus. Various pertinent experiments have been designed such that the facility can be utilized immediately upon completion. Also, analysis of the stiff arm testing procedures and equipment has been performed to help characterize the transient loading on TVC actuators of the shuttle main engines.

Efforts on health monitoring and fault diagnosis have advanced significantly since the semi-annual report. A heuristic form of adaptive Kalman filtering is currently under study with promising results thus far. In fact, hardware design is underway for a more rigorous proof of concept. This technology is expected to significantly impact future efforts on adaptive control as well as allowing the prediction and classification of impending failures in classically controlled actuator systems. Specific details on this work are presented.

The following individuals have been involved in this project:

- 1) Tim A. Haskew, Project Director, Co-Principal Investigator
Assistant Professor, Department of Electrical Engineering
- 2) John Wander, Co-Principal Investigator
Assistant Professor, Department of Mechanical Engineering
- 3) Thomas E. Salem
Ph.D. Student, Department of Electrical Engineering
- 4) Stuart Payne
M.S. Student, Department of Mechanical Engineering
- 5) Ramomohan Challa
M.S. Student, Department of Computer Science
- 6) Sumit K. Bhattacharyya
M.S. Student, Department of Electrical Engineering

- 7) Kris Cozart
M.S. Student, Department of Mechanical Engineering
- 8) Yoon Gyeong Sung
Ph.D. Student, Department of Mechanical Engineering

Thomas Salem completed his masters degree with a thesis on motor selection, and has returned to pursue the Ph.D. degree. In addition to the faculty and graduate student members of the EMA research group listed above, several undergraduates have been involved in associated projects such as software design for a data acquisition system. The group holds weekly meetings where students are encouraged to present their work. This project has not only provided the opportunity for faculty members to be engaged in development of state-of-the-art technology, but it has also allowed students to learn to interact with other engineers in a multi-disciplinary sense. Furthermore, through making public presentations, the students are gaining valuable skills for use in their careers.

Overall, we feel that the first year of this project has been quite successful. We are now to the point where we are comfortable with beginning technology transfer through journal article publication. We expect the submission of at least two papers prior to the next semi-annual progress report. As presented in our renewal for year two, we have substantial plans for upcoming efforts. We will continue to refocus our efforts as requested to meet the immediate needs at MSFC.

II. PHASE 1 TASK I.1: EMA MODELING AND TEST STAND DEVELOPMENT

Several different modeling tasks have been pursued during the first year of this grant. A review of basic modeling formulations and design issues was presented in the midyear report. Also in that report it was indicated that experimental apparatus was needed if more accurate models of roller screw based EMAs were to be developed. An initial design of a test stand was presented and is currently being used to direct construction. While waiting for the test stand to become available, attention has been focused on overall system models that will predict TVC EMA performance and will help guide the development of EMA control algorithms and stiff-arms for TTB hot fire tests. Results to date have produced an EMA control system with force feedback that is similar to that of the hydraulic actuator, analysis of response to nozzle transients using the same actuator models used for control design, and support for the validity of this same model through its ability to predict the data obtained from the stiff-arm tests. Experimental modeling work will begin as soon as the test stand is complete.

II.1. Development of EMA Test Facility

One result of the first year's effort is the detailed design of a general purpose EMA test facility. A supplemental proposal to build this facility at The University of Alabama has been submitted to NASA Marshall Space Flight Center and is reproduced in Appendix A. Those detailed drawings completed to date appear in Appendix B. The test facility will be located in the electric machines lab of the East Engineering Building. Such a location will provide a variety of electrical power supply options to facilitate the testing of different electrical motors in the EMAs. The existing heavy equipment mounting stations will be used to support the test frame and hydraulic load

application equipment. The only site improvements required will be the addition of some storage cabinets and a chain link fence to isolate the test facility from the remainder of the lab.

The following test capabilities should be available once the test stand is completed:

- transient axial loading of up to 100,000 lbf at 6 Hz,
- passive transverse loading of 1000 lbf at 6 in/s travel against 30,000 lbf load,
- measurement of applied torques and motions to identify friction behaviors,
- multiple coupling options between actuators and screws,
- mounting of a roller screw or an entire SME TVC actuator, and
- application of a controlled environment to the actuator.

II.2. Preliminary Experiment Schedule for SSME EMAs

Though the test stand is designed to allow study of a variety of EMAs for a variety of applications, analysis of the TVC EMA's response to SSME startup and shutdown transients is a prime concern. For this reason, a roller screw will be obtained from NASA Marshall and used with a suite of experiments designed to learn about roller screw behavior in general and response to transient disturbances specifically. Stiff-arm tests on the TTB, discussed in more detail in the following section, are scheduled for late 1993 to further identify the nature of these transients. Available data suggests that an actuator that exhibits a significant impedance to output disturbance will cause the excitation of structural resonance and experience shock loads up to 100,000 lbf during these transients [II.1].

The behavior of a roller screw while being backdriven is not entirely understood. The manufacturer of the roller screws being used in the NASA EMA prototypes, SKF, suggests that "Planetary roller screws are reversible under almost all conditions." [II.2] One concern is that though able to be backdriven, they will exhibit unacceptably large impedance to shock-type output disturbance. Another critical concern is over the

health of the bearing if it is subjected to the shock loading expected. Therefore, the most critical experiment to be performed will be the application of transient loading profiles established by the stiff-arm tests. These loads will be produced by a force controlled hydraulic actuation system. Because damage to the roller screw may result from this experiment, several lower energy experiments will be scheduled in rapid succession before the transient loading experiments are performed.

Transverse loading experiments will be performed to verify that the roller screw will not be damaged by transverse loads in excess of 10% of axial load. These experiments will be conducted by compressing a spring in series with a load cell transverse to the axis of the roller screw. This assembly supports the nut and rides on a linear bearing along the axis of the screw. The screw will be turned by a direct drive motor to drive the nut back and forth over different sections of the screw under different combinations of transverse and axial load. The number of cycles will far exceed the duty cycle associated with the TVC application. Bearing wear will then be determined and will hopefully indicate that transverse loading is not a primary concern.

Friction modeling experiments will be performed with much the same configuration. The direct drive motor allows one estimate of the applied torque to be obtained by measurement of motor current. In addition, axial load and actual applied torque will be measured as well as nut reaction torque. These measurements will be performed with the screw driven by the motor and being backdriven under mild loading conditions by hydraulic actuation. Friction models appropriate for both angular and linear drive conditions will be developed. These models will be very useful in developing control algorithms for the TVC application and other EMA applications.

Bearing performance under the expected TVC duty cycle will also be determined by driving the roller screw through representative motion profiles while varying the load with the hydraulic force control system. Here again, the test is expected to be non destructive and will be performed before the transient loading experiments. Later in

the project, a similar simulated launch duty cycle will be used to study motor and gear reduction choices, fault detection algorithms, and control designs. Other EMA application prototypes will also be tested.

II.3. Analysis for Design of Stiff-Arm SSME Tests

The transients associated with engine startup and shutdown have been studied using the TTB test stand by substituting spring-loaded supports for the TVC actuators during hot fire tests. Loading information has been inferred from strain measurements taken from the body of the "stiff-arm" support. Though there is some concern that this data is not accurate, there is indication of a transient oscillatory response in the stiff-arm of up to 80,000 lbf at a frequency of roughly 6 Hz. These tests have been used to direct the investigation of roller screw behavior when subjected to a 100,000 lbf shock load. At the same time, an effort is under way to verify the results of previous tests. One improvement in the instrumentation to be made is the direct measurement of load by the inclusion of in-line force sensors. Though the actual load on the stiff-arm will now be measured, two important questions remain to be answered while planning the tests. Most importantly, since the loads applied to the actuator (not the stiff-arm) are the real concern, tests should be performed that provide information suited for extrapolating to actuator loads. What kind of tests are best suited for such extrapolation? This first question leads to the second: will the hysteretic nonlinearity inherent in the parallel stacks of disk springs used in the stiff-arm make extrapolation and/or identification of the force applied to the nozzle difficult? [II.3] The force/strain calibration experiments performed on previously used stiff-arms seem to indicate less of a hysteretic effect that is suggested by sales literature.

Force/deflection tests with the newly designed stiff-arm will be conducted in order to calibrate the arm and develop a dynamic model of the arm. These tests will also provide additional indication of the degree of hysteresis exhibited by the arm. A

numerical model of a disk spring has been developed in order to simulate stiff-arm behavior and to help answer the important questions raised above. Engineering data taken from the sales literature [II.2] is reproduced in Figure II.1 below. Similar results are produced by the disk spring model as shown in Figure II.2. The disk spring model is implemented in MATLAB and will be used with a detailed numerical simulation model of the stiff-arm and the SSME in order to predict experiment behavior and to determine whether nozzle force can be predicted by actuator force. The validity of this study will be primarily limited by the quality of the structural model of the SSME used in the study. Some degree of confidence in the usefulness of the model presented by Lominick for control design is indicated by the fact that when the actuator portion of the model is replaced by a simple linear spring model of the stiff arm used in previous TTB hot fire tests a natural frequency of 6 Hz is predicted. This seems to be the dominant frequency present in the test data resulting from previous TTB tests [II.1].

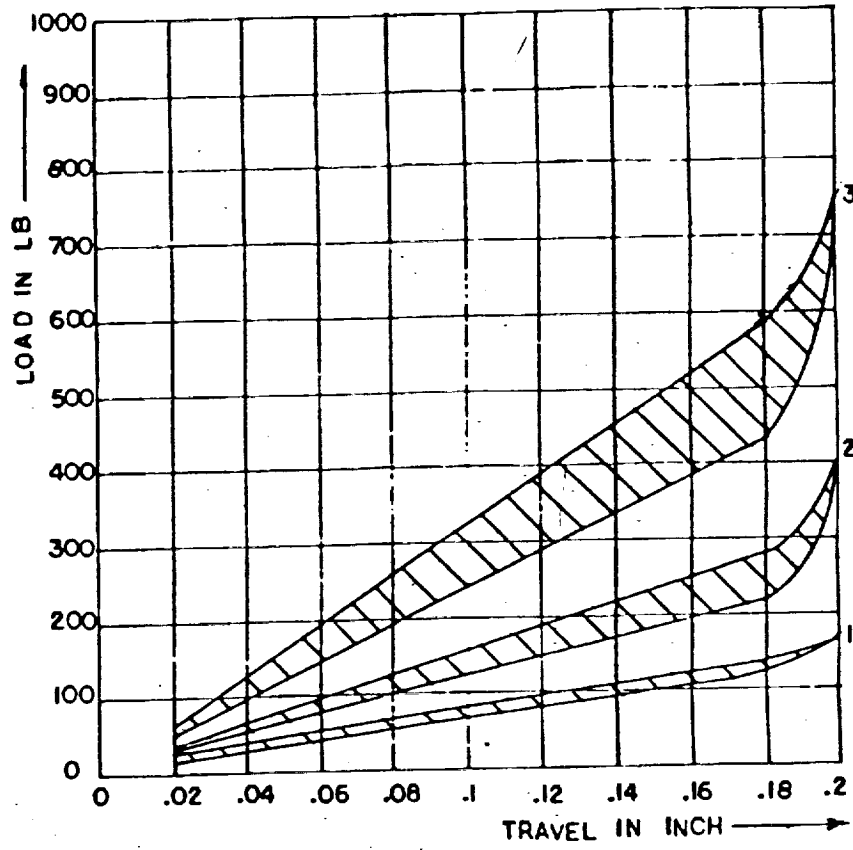


Figure II.1. Published Disk Spring Behavior. [II.2]

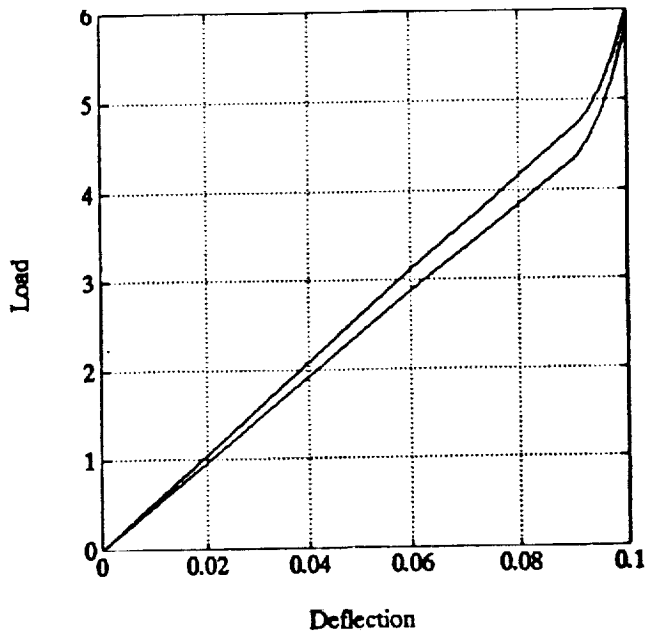


Figure II.2. Numerically Generated Disk Spring Model Behavior.

II.4. Development of SSME TVC with an EMA Similar to Previous Control with a Hydraulic Actuator.

This section presents an initial study of control options for the EMA. The study is a comparison of linear, small signal designs to those presented for the existing hydraulic actuator by Jim Lominick [II.4]. The analysis presented in the original control design is extended to include consideration of the system response to force disturbances on the engine nozzle.

Figure II.3 illustrates in schematic the two different systems as modeled for the control design. The schematic of the hydraulic system is taken from Lominick [II.4]. The essential modeling differences can be illustrated by the bond graphs shown in Figure II.4. In the bond graphs, C's represent compliance, I's represent inertia and the 1's and 0's (called junctions) represent constraints between system variables. The S's represent sources of power including the main control input, bypass control, and force applied to the nozzle. Though the hydraulic fluid in the existing actuator stores some kinetic energy, it is considered only as a potential energy storage in the control model as indicated by the C on the 0 under the bypass loop. Since there may be significant rotational energy associated with the linear motion of the actuator, kinetic energy storage in the actuator should be considered with the EMA. On the other hand, the EMA might be made stiff enough so that potential energy storage can be ignored. Since the hydraulic actuator was significantly more stiff than either the mounting point or the nozzle, omission of actuator stiffness should not change system response significantly. The signal diagrams of the feedback loops and associated effective signal dynamics given by Lominick do not provide as complete a physical model as do the other system parameters but is sufficient to allow comparison with EMA response. In addition to the results presented below based on this simple model, a more accurate model of the EMA system will be used to develop more accurate response prediction.

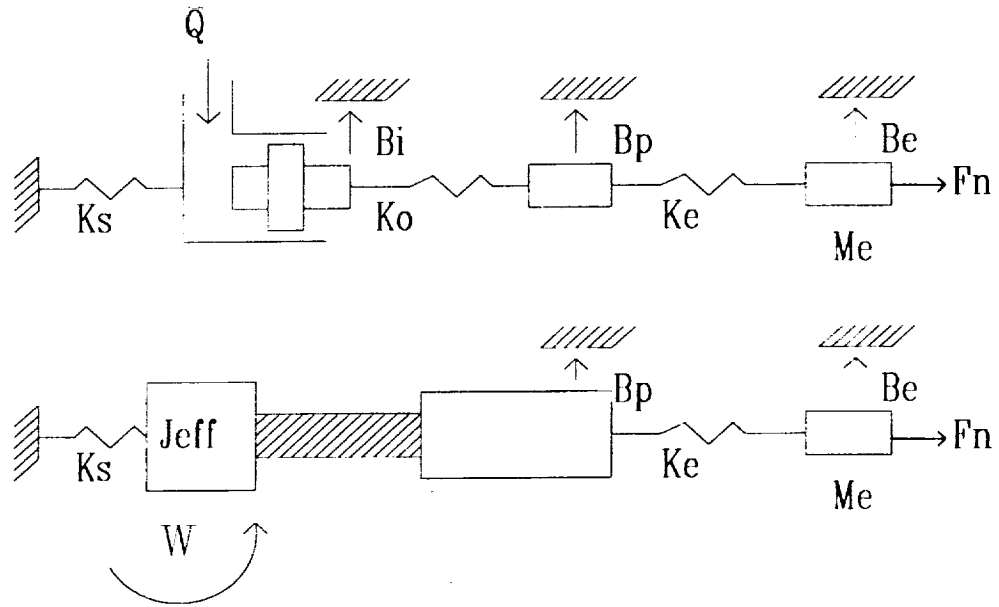


Figure II.3. Schematics for Hydraulic and Electro-Mechanical TVC Actuators.

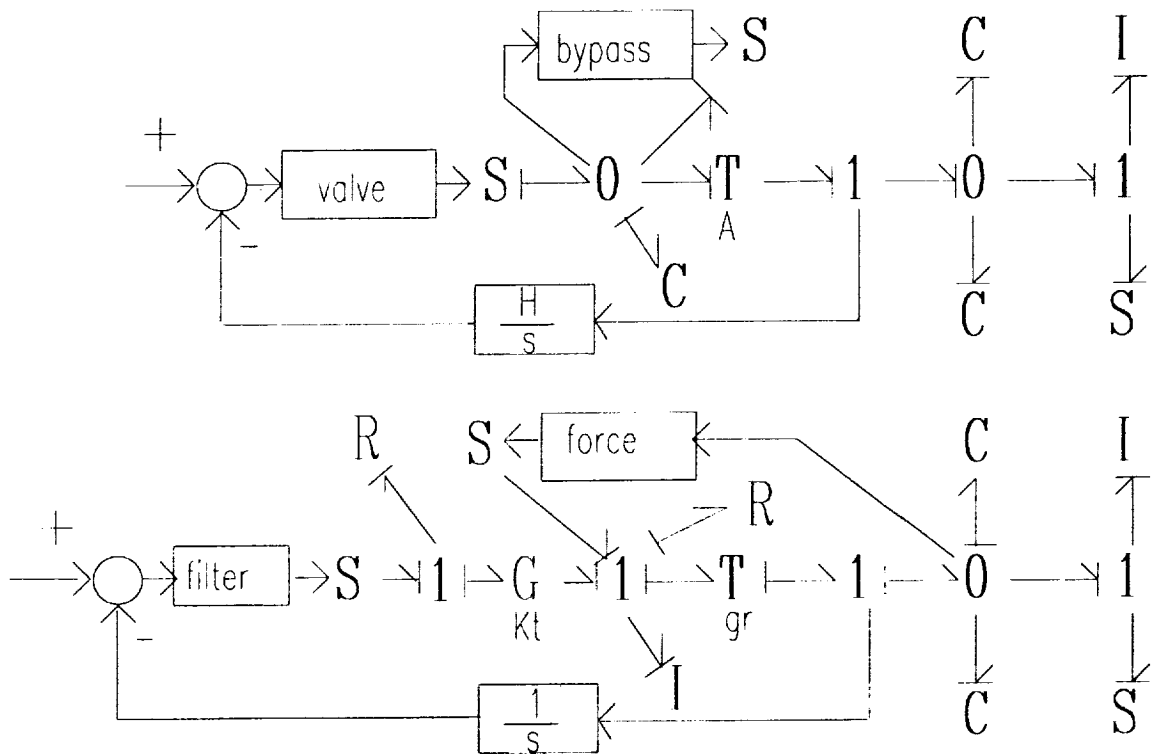


Figure II.4. Bond Graph Modeling Comparison Between Hydraulic Actuator and
EMA.

The design goals for the development of the actuator control were:

- produce a phase lag of less than 20 degrees at 1 Hz, and
- minimize the integral square error of nozzle position minus command for a step input.

A bode plot of output position versus command for the current design is reproduced from Lominick in Figure II.5. The system model presented in [II.3] was used to generate the bode plot of actuator force versus the disturbance force applied to the nozzle shown in Figure II.6. This frequency response function is of primary concern when considering the startup transient. In fact, if the control loops are eliminated and the stiffness of the hydraulic oil is replaced by a model of the stiff-arm, a model of the stiff-arm test situation is produced.

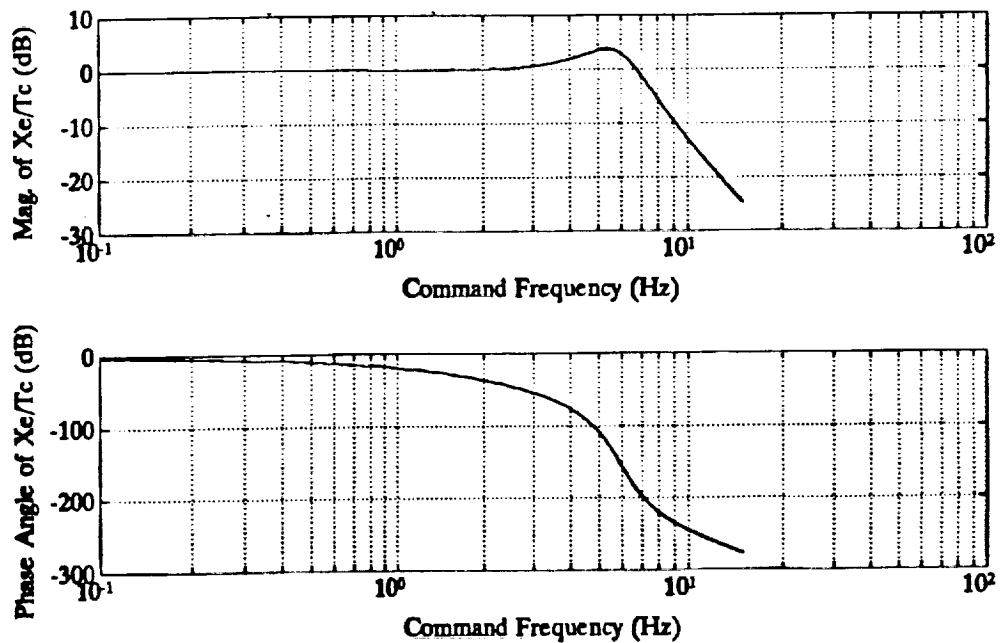


Figure II.5. Bode Plot of SSME Response with Existing Hydraulic Actuator.

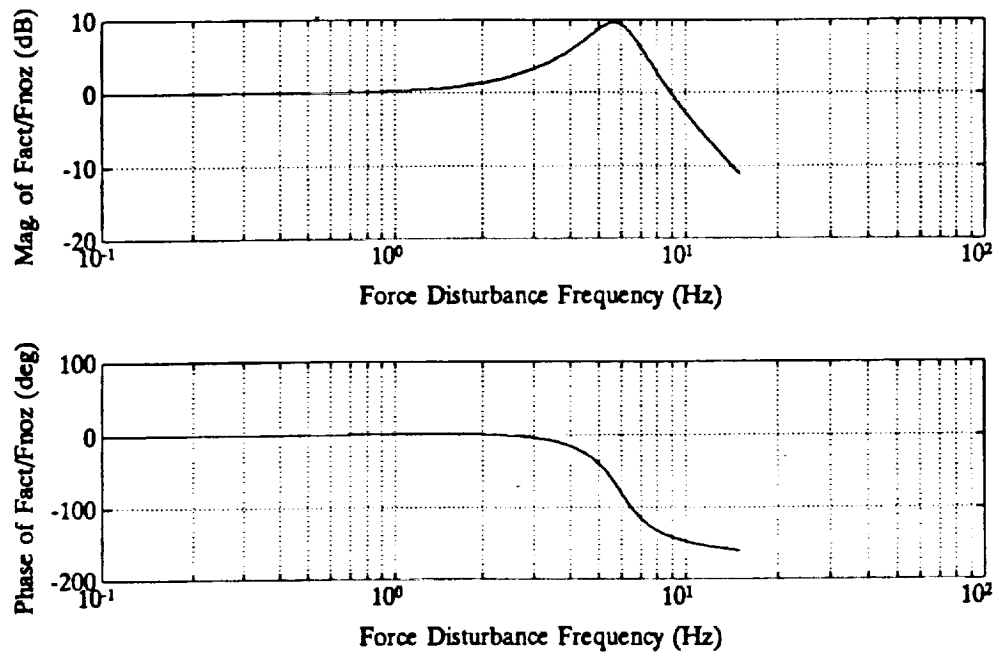


Figure II.6. Response of Existing Hydraulic System to SSME Force Disturbance

With physical parameters taken from the NASA EMA prototyping effort and the electrical effects associated with power supply and motor inductance ignored, a control system design analogous to the hydraulic design produces the results shown by the dashed line in the following figures. The existing hydraulic actuator's performance is plotted with a solid line for comparison. The EMA response shown in these plots was obtained with a compensator in the forward loop and the bypass loop of the hydraulic system replaced with a force feedback loop. No dynamics have been ascribed to the force sensor itself and no additional compliance has been considered due to the sensor. If such effects are made significant by the choice of a particular force sensor they could easily be added to the model. Though the design parameters for this control structure have not been optimized, it is apparent that the response to command can be made to have similar frequency characteristics and that the actuator load resulting from nozzle disturbance can be significantly reduced. The response to a step position command exhibits somewhat greater overshoot but quicker settling.

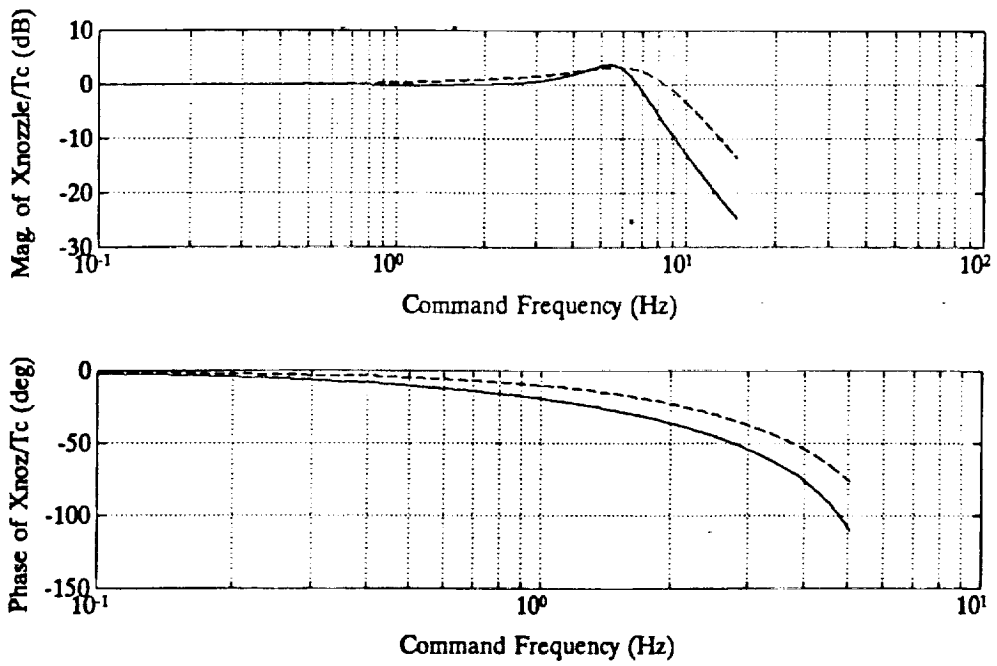


Figure II.7. Comparison of Position Control Response

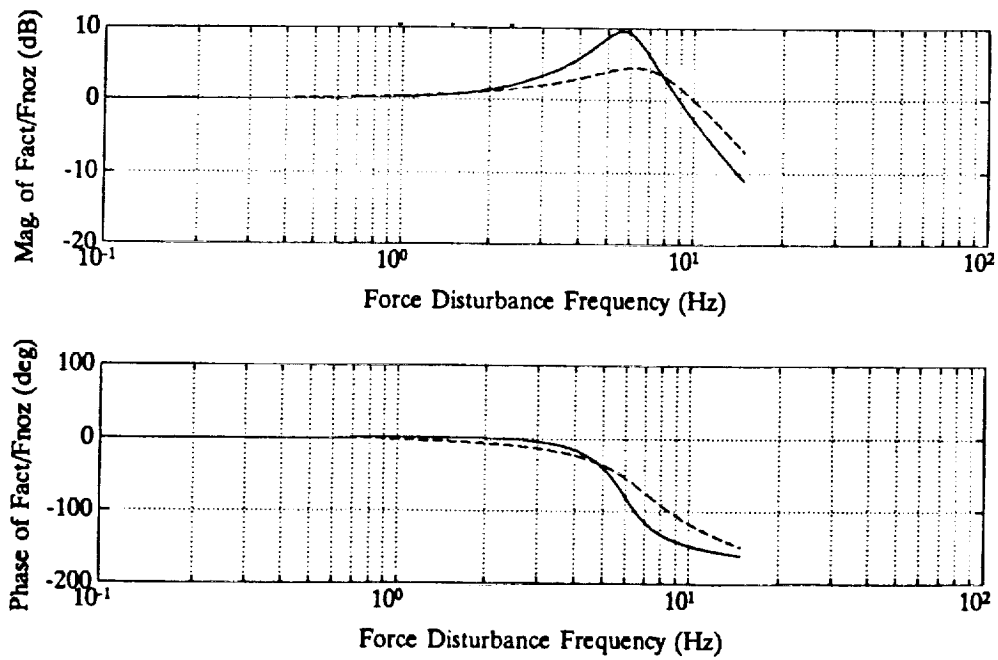


Figure II.8. Comparison of Response to Nozzle Disturbance

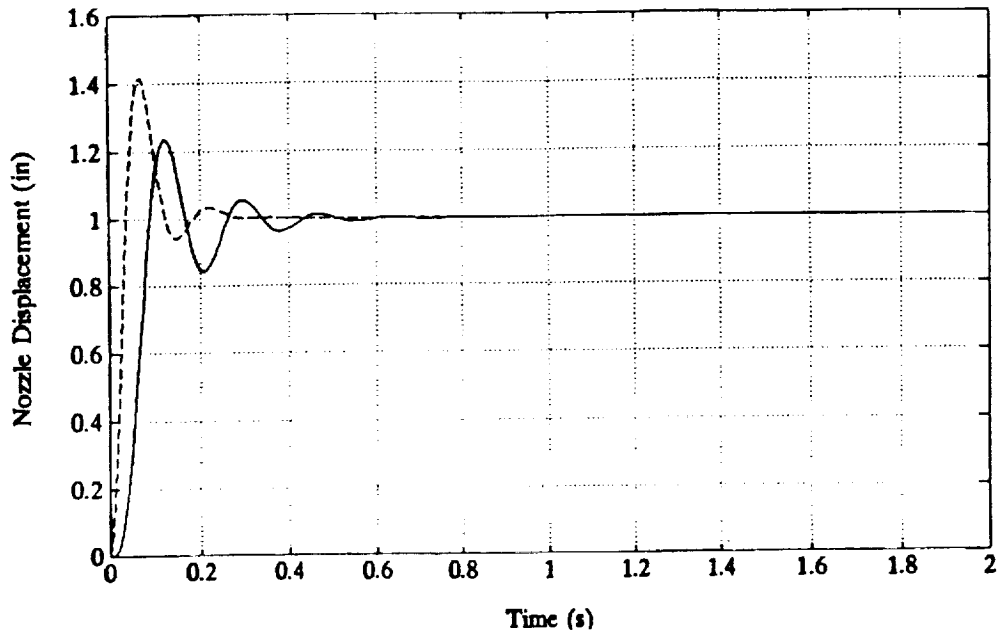


Figure II.9. Comparison of Time Response to Step Change in Command

The possibility of removing the force feedback loop from the control system and accommodating the nozzle disturbance passively was considered. Since the limitation on prime mover torque generating capability and its relationship to rotor inertia is not clear at this time, reasonable assumptions on gear reduction and rotating inertia have been made based on general motor properties. Given a specific motor and duty specification, exact parameter values could be used for this analysis. Figure II.10 shows the passive (uncontrolled) force response of the EMA to nozzle disturbance for both a reasonable parameter set (solid line) and one that includes gear reductions and rotor inertias that are lower than are likely to satisfy the SSME TVC load requirements (dashed line). One can see that the load necessary to backdrive the rotary inertia is sufficient to excite the mechanical resonance even if unreasonably small parameter values are used. Initial indication is that a force feedback loop in the EMA should be implemented to take the place of the bypass loop in the hydraulic actuator.

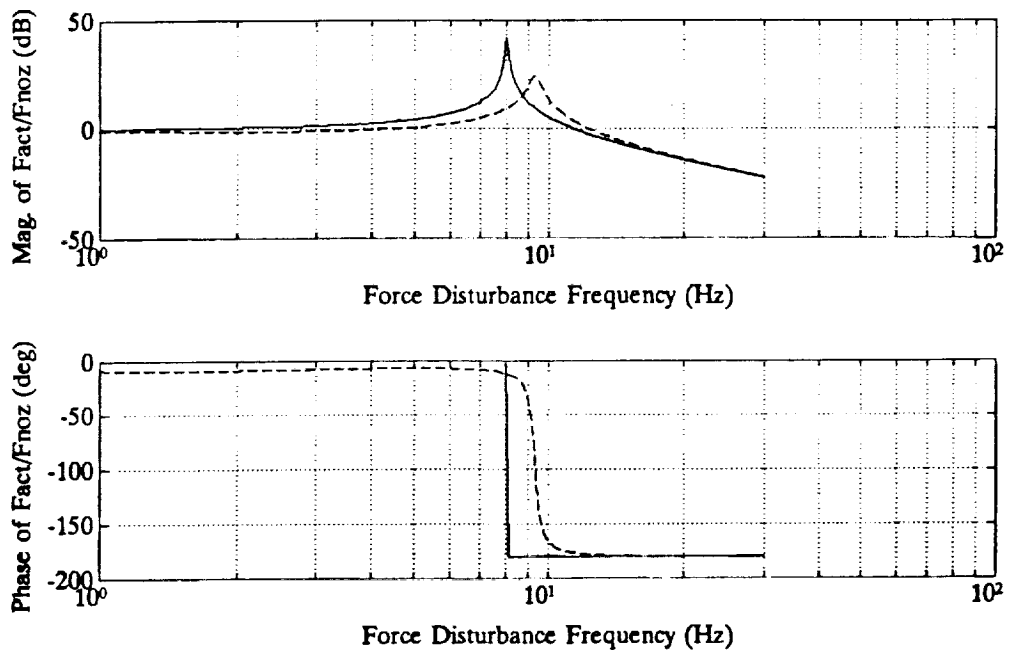


Figure II.10. Actuator Load Responses To Nozzle Disturbance Without Force Feedback

II.5 References

- [II.1] Strain Gauge Measurement of Stiff Arm Transient Load During TTB Test 19,
Memo of October 30, 1990 from Eric Earhart to John Harbison.
- [II.2] SKF Planetary and Recirculating Roller Screws, Catalogue 3793 U.S., SKF Group,
1990.
- [II.3] National Disk Springs, Catalogue 991, Rolex Company, 1983.
- [II.4] Design and Optimization of SSME TVC System, Memo of October 17, 1973 from
Jim Lominick to Charlie Cornelius.

III. HEALTH MONITORING AND FAULT DIAGNOSIS

In this report section, our efforts in health monitoring and fault diagnosis are presented. Presently, we are focusing solely on the thrust vector control (TVC) actuator driven by a brushless dc machine (BDCM) operating under PWM control. While this will be discussed in general terms, the majority of the technical content will be aimed at the separately excited brushed dc motor (SEDM).

The SEDM exhibits operational characteristics virtually identical to those of the BDCM. However, it provides far less complexity than the BDCM. Thus, the SEDM was chosen for a feasibility study and to refine the basic algorithms to be used.

III.1. Fundamental Philosophy

The fundamental philosophy governing our approach to health monitoring and fault diagnosis is to assimilate measurements from the actuator and process this data to provide an estimate of the system state as well as a trajectory of system parameters. While it is yet to be proven, we are assuming that each fault mode of interest will have a unique signature to be found in the state estimates and parameter trajectories. In addition to using parametric values to establish fault modes, they can be used as feedback in various adaptive control system implementations [III.1, III.2, III.3].

The list of fault modes presently under consideration for the BDCM includes: winding open-circuits, winding short-circuits (phase-to-phase and phase-to-ground), bearing degradation, and rotor flux weakening. While this list is not exhaustive, it does provide a logical starting point. Rotor flux weakening in the BDCM is equivalent to a field current reduction in the SEDM. Thus, as the SEDM was chosen as the starting point for analysis, the initial fault for consideration was chosen to be flux weakening. Detailed results will be presented.

III.2. The Kalman Filter

The Kalman filter is a proven and widely used tool for processing noisy measurements from a dynamic system to provide an optimal estimate of the system state. We will now introduce some of the fundamentals of Kalman filtering that have been applied to our problem. An excellent derivation and discussion on the filtering topic can be found in [III.4]. Let us assume that a dynamic system can be described by the set of first order linear differential equations shown in matrix form in (III.1).

$$\dot{\mathbf{x}} = [\mathbf{A}]\mathbf{x} + [\mathbf{B}]\mathbf{u} \quad (\text{III.1})$$

In (III.1), \mathbf{x} is the state vector, \mathbf{u} is the input or forcing function vector, and \mathbf{A} and \mathbf{B} are constant coefficient matrices with entries defined by the system parameter. The dot notation indicates the time derivative.

For constant or known inputs if a clamped state variable response is adequate [III.5], the state equations of (III.1) can be written in homogenous form as shown in (III.2).

$$\dot{\mathbf{y}} = [\mathbf{C}]\mathbf{y} \quad (\text{III.2})$$

In (III.2), \mathbf{y} is an augmented state vector as defined in (III.3) and \mathbf{C} is a constant coefficient matrix as defined in (III.4).

$$\mathbf{y} = \begin{bmatrix} \mathbf{x} \\ \mathbf{u} \end{bmatrix} \quad (\text{III.3})$$

$$[\mathbf{C}] = \begin{bmatrix} \mathbf{A} & \mathbf{B} \\ \mathbf{0} & \mathbf{0} \end{bmatrix} \quad (\text{III.4})$$

The solution to the homogeneous equations of (III.2) can be found at distinct points in time by use of the state transition matrix Φ . This is illustrated in (III.5) where state vector subscripts indicate evaluation at distinct points in time.

$$y_{k+1} = [\Phi]y_k + w_k \quad (III.5)$$

In (III.5), w is a vector of noise introduced into the process. This term has serious implications to be presented later.

The measurements obtained from the system can be placed in a vector z . Since the measurements will be obtained by sampling (for a digital system) at discrete points in time, the same subscript notation used for the state vector will be employed. Let us constrain ourselves to the case where the measurements are linear combinations of the states. Thus, the measurement vector can be expressed as a function of the states as indicated in (III.6), where H is a constant coefficient matrix.

$$z_k = [H]x_k + v_k \quad (III.6)$$

In (III.6), v is a vector of noise introduced into the measurements.

Expressions (III.5) and (III.6) are in the form required for use of the Kalman filter. The filter assimilates measurements and estimates the system states in a recursive manner. We begin with the assumption that the noise in the process as well as the noise in the measurements are white and uncorrelated sequences with known covariance structures. This assumption is not as limiting as it may appear. The covariance matrix for the process noise, w , will be defined as Q . The covariance matrix for the measurement noise, v , will be defined as R .

We begin with an *a priori* estimate of the system state at some time k , y_k^- . The super minus indicates that this estimate is prior to assimilation of the measurement at time k . Additionally, we assume that the covariance matrix, $[P_k^-]$, of the estimate error vector (actual state minus estimated state) is known. This covariance matrix is typically the null matrix when the initial conditions of system are known.

When the measurements are taken at time k , the state vector is estimated as a linear combination of the *a priori* estimate and the difference between the measurements and expected measurements as indicated in (III.7)

$$\hat{y}_k = y_k^- + [K_k] \{z_k - [H]y_k^-\} \quad (III.7)$$

In (III.7), K is the Kalman gain matrix, as defined in (III.8).

$$[K_k] = [P_k^-][H]^T \{[H][P_k^-][H]^T + [R]\}^{-1} \quad (III.8)$$

In the case where the initial conditions of the state vector are known, the P matrix for $k=0$ will be the null matrix. Thus, Kalman gain matrix will be null. As a result, (III.7) will yield an estimated state exactly equal to that provided as initial conditions. As estimation proceeds through many time steps, more emphasis will be placed on the measurements.

Following estimation of the system state, the error covariance matrix can be updated as indicated in (III.9), where I is the identity matrix.

$$[P_k] = \{[I] - [K_k][H]\} [P_k^-] \quad (III.9)$$

The error covariance matrix is projected ahead to the instant of the next measurement assimilation as shown in (III.10).

$$\left[P_{k+1}^- \right] = [\Phi][P_k][\Phi]^T + [Q] \quad (\text{III.10})$$

Similarly, the estimated state is projected ahead to produce the *a priori* estimate needed for the next pass through the filter loop. This is illustrated in (III.11).

$$\mathbf{x}_{k+1}^- = [\Phi]\hat{\mathbf{x}}_k \quad (\text{III.11})$$

Notice that the Kalman filter loop is strongly dependent on knowledge of the system parameters for evaluation of the state transition matrix. Additionally, the filter appears strongly dependent on exact noise descriptions. However, the filter is quite robust even when noise is poorly modeled. We will consider application of the Kalman filter to the SEDM.

III.2.1. The Separately Excited DC Machine

The separately excited dc machine equivalent circuit is shown in Figure III.1 [III.6].

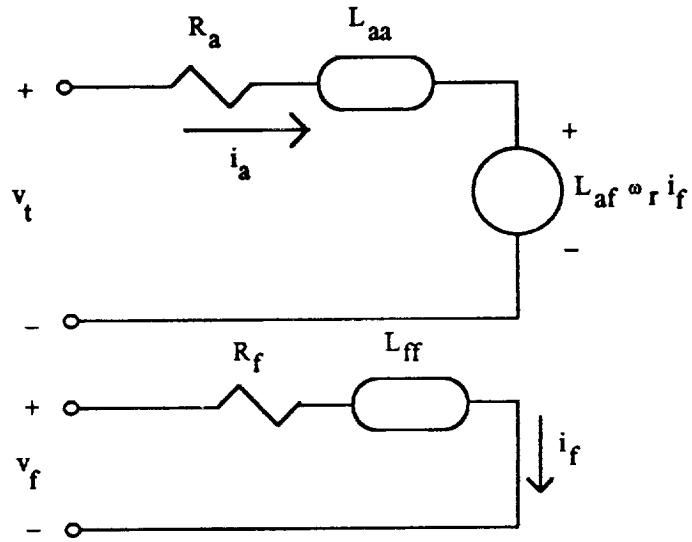


Figure III.1. Separately Excited DC Machine Circuit Model.

We will assume that the field voltage is constant. This assumption most accurately represents nominal conditions in the BDCM, constant rotor flux.

The developed torque in the machine is given in (III.12).

$$T_{\text{dev}} = L_{\text{af}} i_f i_a \quad (\text{III.12})$$

Note that the product of field current and armature to field mutual inductance occurs in expressions for both the back emf and the developed torque. Thus, we make the definition in (III.13) which leads to (III.14) and (III.15).

$$k_m = L_{\text{af}} i_f \quad (\text{III.13})$$

$$e_a = k_m \omega_r \quad (\text{III.14})$$

$$T_{\text{dev}} = k_m i_a \quad (\text{III.15})$$

Above, e_a is the back emf and ω_r is the mechanical speed of the rotor.

For the purposes at hand, the mechanical load on the shaft was treated as a constant, T_L . This leads to the equation of motion presented in (III.16).

$$T_{dev} - T_L = J \frac{d\omega}{dt} + b\omega \quad (III.16)$$

J is the moment of inertia of the machine rotor and load, and b is the damping coefficient.

The state equations for the system are provided in (III.17).

$$\frac{d}{dt} \begin{bmatrix} i_a \\ \omega_r \end{bmatrix} = \begin{bmatrix} -\frac{R_a}{L_{aa}} & -\frac{k_m}{L_{aa}} \\ \frac{k_m}{J} & -\frac{b}{J} \end{bmatrix} \begin{bmatrix} i_a \\ \omega_r \end{bmatrix} + \begin{bmatrix} \frac{1}{L_{aa}} & 0 \\ 0 & -\frac{1}{J} \end{bmatrix} \begin{bmatrix} v_t \\ T_L \end{bmatrix}$$

$$\dot{\mathbf{x}} = [\mathbf{A}]\mathbf{x} + [\mathbf{B}]\mathbf{u} \quad (III.17)$$

These state equations can be converted to homogeneous form as previously indicated. These equations were coded into a finite-difference simulation program. The measurements taken were the armature current and rotor speed. The terminal voltage and load torque were treated as pseudo-measurements. The simulation program produced the actual values of the measured quantities. Onto these signals, noise was injected. We now examine the performance of the Kalman filter.

III.2.2. Application of the Kalman Filter

The Kalman filter was applied to measurements taken from simulating a 200 Hp dc machine with the following parameters [III.6]:

$$R_a = 0.012\Omega, L_{aa} = 0.35\text{mH}$$

$$R_f = 12\Omega, L_{ff} = 9\text{H}$$

$$L_{af} = 0.18\text{H}$$

The moment of inertia was 30 kg-m². The damping coefficient was neglected. The field and terminal voltages were equal at 250 V, and the load torque was 2375 N-m.

The machine was simulated from starting to steady-state. The noise injected onto the current signal had zero mean and a standard deviation of 125 A. The noise injected onto the speed signal had zero mean and a standard deviation of 6.25 rad/s. Figure III.2 shows the actual signal, noisy signal, and estimated signal for the armature current. Figure III.3 shows similar data for the motor speed. Note that the actual and estimated signals are coincident for both the armature current and the rotor speed. In this example, no noise was considered in the process, only the measurements.

III.3. Use of the Kalman Filter for Health Monitoring and Fault Diagnosis

Previously, we illustrated accuracy of the Kalman filter for estimating the state of the SEDM in the case where the system parameters were at nominal values. This property may prove useful for eliminating noise contamination in feedback signal. However, this is not helpful for health monitoring and fault diagnosis. The presence of a system fault will be detectable by variations in the system parameters. Thus, our filter must be able to operate accurately over a wide range of parametric values.

Figure III.2. Armature Current.

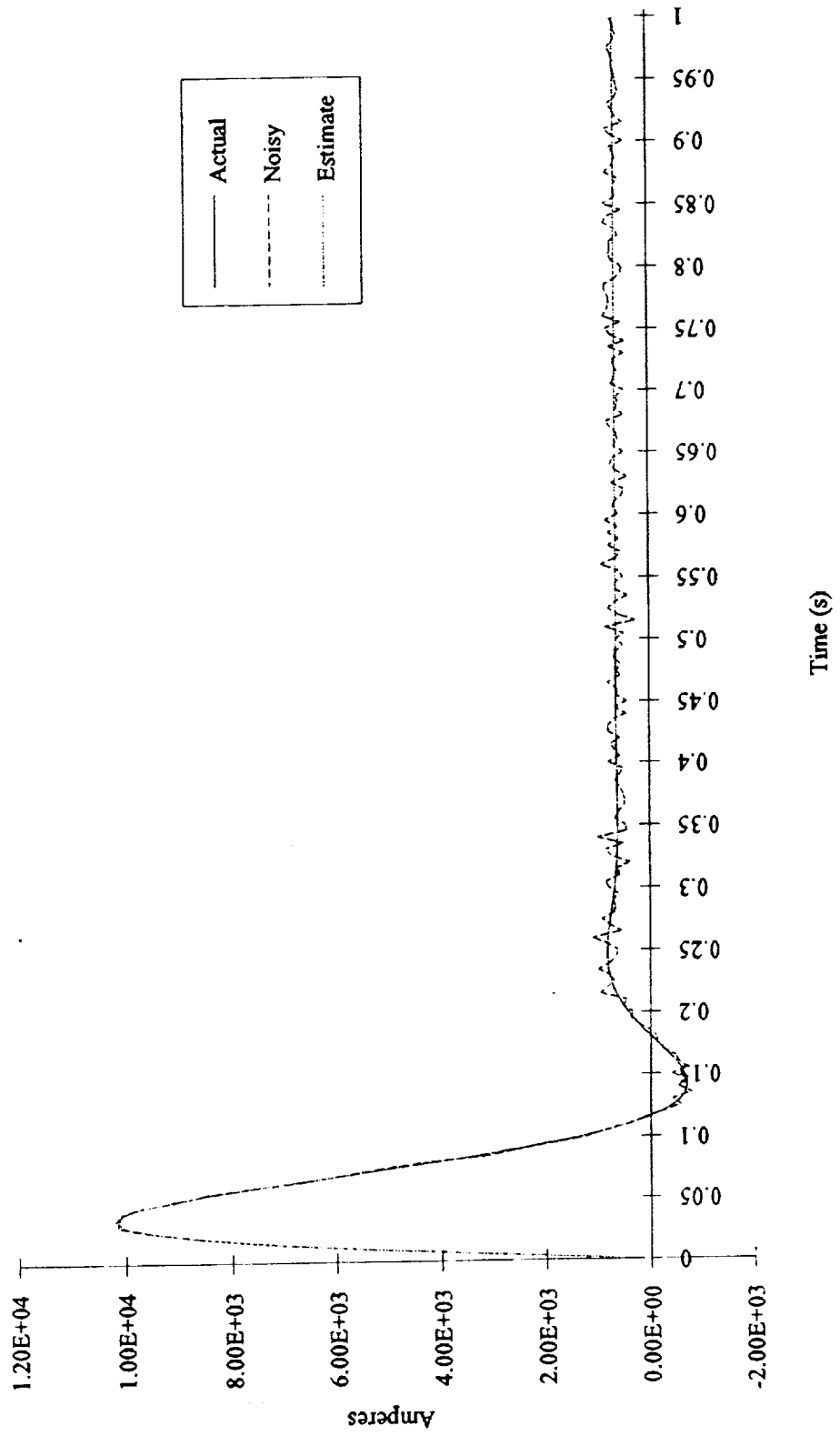
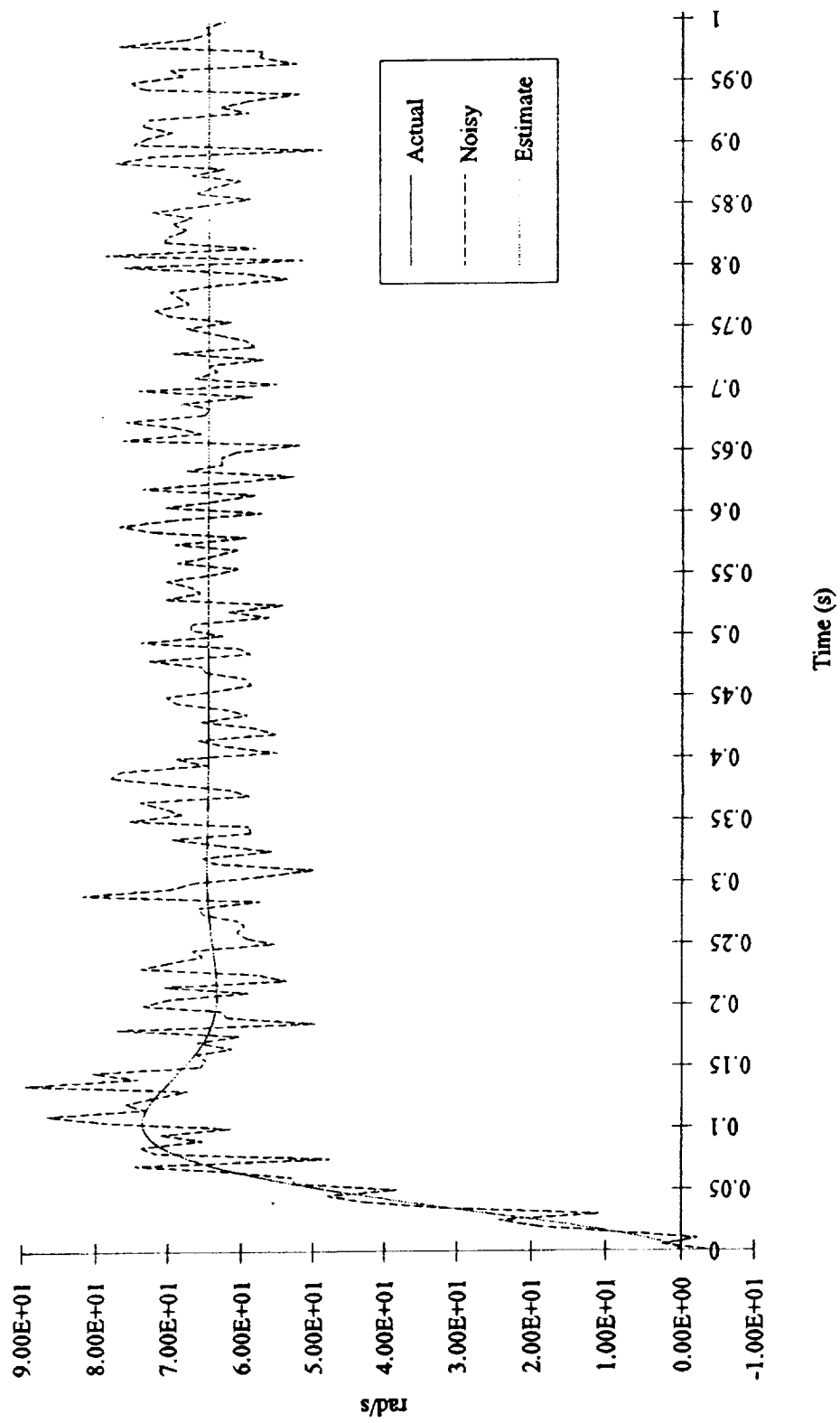


Figure III.3. Mechanical Rotor Speed.



The shortcomings of the filter when parameters are changed are best illustrated by example. Consider the previously presented machine operating in steady state when the field current is reduced to 70% of the pre-disturbance value at a time of 0.25s. This situation is analogous to a step decrease of rotor flux in the BDCM. Figure III.4 shows the result for the armature current. Notice that the filter continues to track the pre-disturbance state. This does not provide adequate noise filtration for feedback, nor does it predict that some type of fault has occurred.

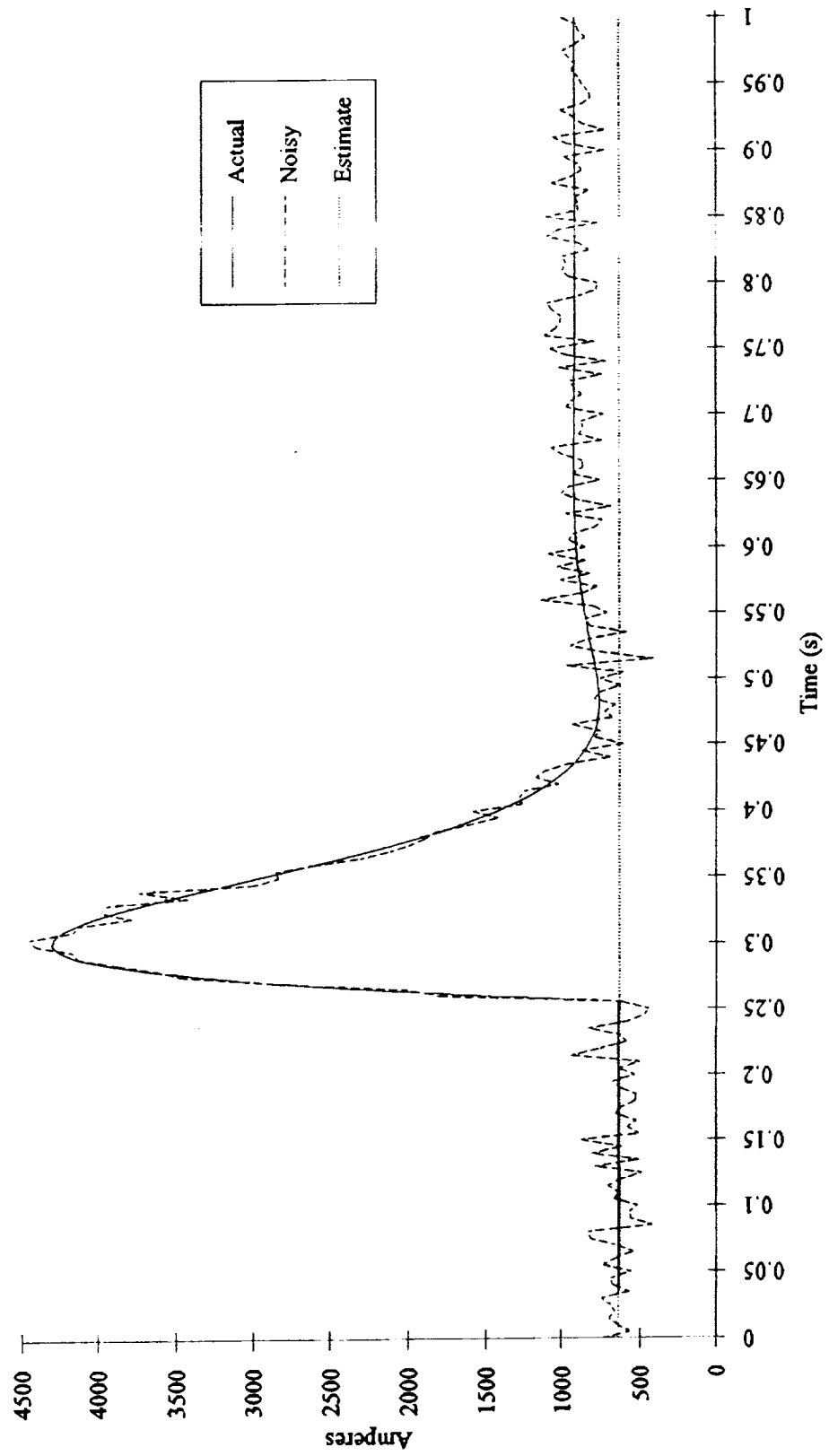
However, the performance of the filter does lend credence a valuable finding of others [III.7]. The large swing in armature current measurement did not drastically impact the estimate, which implies that pulse width modulation strategies producing wide variations in voltage and current measurements may be effectively treated as noise about a fundamental frequency. This is also significant in the sense that we need not force sampling rates that will entirely allow reconstruction of the current waveforms. In fact, we will be interested in average values.

The question then, is how to utilize the Kalman filter in such a way as to monitor motor health and adequately detect faults. This actually reduces to the question of how to utilize the Kalman filter to accurately estimate the system state and identify system parameters in a dynamic sense. One answer to this question is to use either the linearized or the extended Kalman filter [III.4].

III.3.1. Linearized and Extended Kalman Filters

In applying the linearized or extended Kalman filter, uncertain system parameters, only k_m for our purposes, are considered state variables. This may, and does in our case,

Figure III.4. Armature Current.



make the state model nonlinear. Thus, the state model takes the form indicated in (III.18).

$$\dot{\mathbf{x}} = \mathbf{f}(\mathbf{x}, \mathbf{u}, t) + \mathbf{w} \quad (\text{III.18})$$

In (III.18), \mathbf{f} is a non-linear vector function of the state variables, inputs, and time. As before, \mathbf{w} is process noise. The measurement vector is often defined as a non-linear functions of the states. However, we will maintain the same definition as presented in (III.6). We will assume that we have a nominal trajectory of the states, $\mathbf{x}^*(t)$.

The origin of the nominal trajectory forms the distinction between the linearized and extended Kalman filters. In the linearized case, the nominal trajectory is based on nominal system parameters. In the case of the extended Kalman filter, the nominal trajectory is based on the system parameters computed from the previous estimate. In either case, the nominal trajectory is chosen to satisfy the deterministic differential equation of (III.19).

$$\dot{\mathbf{x}}^* = \mathbf{f}(\mathbf{x}^*, \mathbf{u}, t) \quad (\text{III.19})$$

As system parameters vary with time, the actual system trajectory will deviate from the nominal trajectory. Thus, (III.18) can be rewritten in terms of the nominal trajectory as shown in (III.20).

$$\dot{\mathbf{x}}^* + \Delta\dot{\mathbf{x}} = \mathbf{f}(\mathbf{x}^* + \Delta\mathbf{x}, \mathbf{u}, t) + \mathbf{w} \quad (\text{III.20})$$

Above, Δx is the deviation from the nominal trajectory. The modified measurement equation is presented in (III.21).

$$z = [H](x^* + \Delta x) + v \quad (III.21)$$

Equations (III.20) and (III.21) can be expanded in a Taylor's series. If only the first order terms are retained, the linearized dynamic system and measurement equations presented in (III.22) and (III.23) result.

$$\Delta \dot{x} = \left[\frac{\partial f}{\partial x} \right]_{x=x^*} \Delta x + w \quad (III.22)$$

$$[z - [H]x^*] = [H]\Delta x + v \quad (III.23)$$

These equations are in the same form as required for the linear Kalman filter. In this case, however, the filter provides as output, deviations from the nominal state vector.

While this algorithm appears extremely suitable for detecting fault induced changes in system parameters, it is based on a rather limiting assumption. If only the first order terms of the Taylor's series expansions are retained, deviations from the nominal trajectory are required to be small. Such was appropriate in the case of induction motor rotor time constant estimation as presented in [III.7]. However, this will not likely be the case under faulted conditions. This problem can be overcome by iterating at each estimation phase. However, this will require extensive computational time. Thus, fault detection may be too late. Additionally, by the time a parameter estimate is completed from a given set of measurements, parameters may have changed sufficiently to render output useless in an adaptive control sense. However, work is continuing to adapt this method to something feasible for our needs.

III.3.2. Adaptive Kalman Filtering

The adaptive Kalman filter [III.4] provides a starting point for the method of health monitoring and fault diagnosis that we currently support for use in TVC EMA systems. This filter architecture consists of multiple linear Kalman filters with various system models operating in parallel. The "probability" that each filter is correct is computed based on the measurements and predicted states of each filter. The final estimated state vector is computed as the sum of all filter estimates with each term weighted by the probability of the correctness of that filter. The system parameters can be determined within a reasonable range by analyzing the probabilities associated with each filter. This scheme is illustrated in Figure III.5.

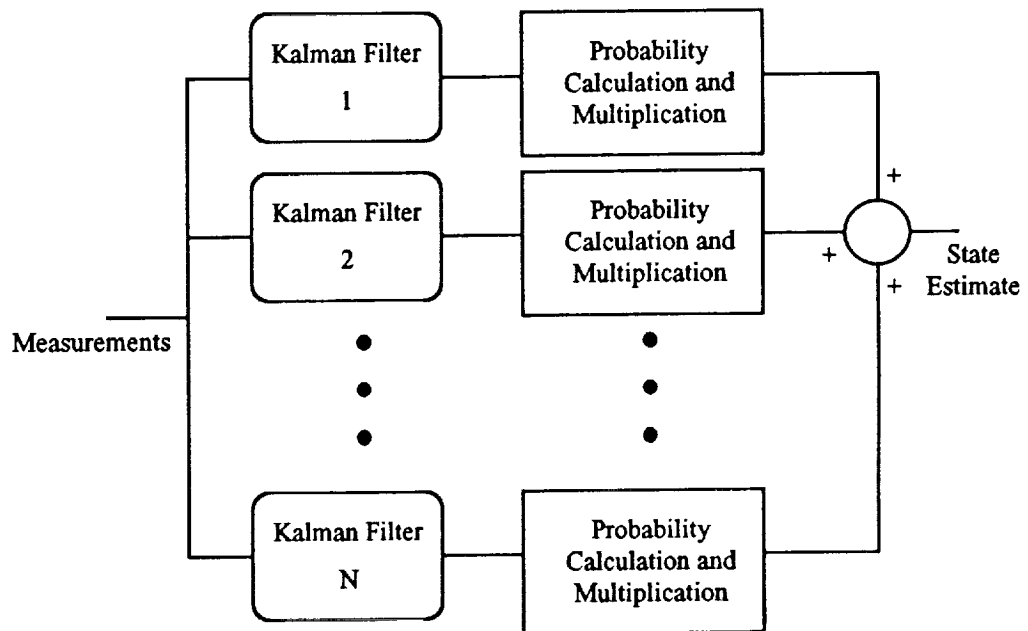


Figure III.5. The Adaptive Kalman Filter.

For predicting a decrease in field current in the SEDM or rotor flux in the BDCM, each of the N Kalman filters would have a different state transition matrix resulting from

computation with different values of flux. In the case of the SEDM, this corresponds to using different values for the motor torque and back-emf constant.

This scheme has been heuristically modified for demonstration on the purpose at hand. Let us define the estimated state at time k from filter j as $\hat{\mathbf{x}}_k(j)$. We also will define the projected state for time $k+1$ from filter j as $\mathbf{x}_{k+1}^-(j)$. The time projection of the state from each filter can be used to compute a projected set of measurements. This calculation is illustrated in (III.24) for filter j .

$$\hat{\mathbf{z}}_{k+1}(j) = [\mathbf{H}] \mathbf{x}_{k+1}^-(j) \quad (\text{III.24})$$

When the new measurements are assimilated, the projected measurements from each filter are compared with the actual measurements. An error for each filter is calculated as the weighted sum of the errors for each measured quantity. This is illustrated for filter j in (III.25).

$$E(j) = [\mathbf{z}_{k+1} - \hat{\mathbf{z}}_{k+1}(j)]^T \{\text{diag}(\mathbf{Q})\} [\mathbf{z}_{k+1} - \hat{\mathbf{z}}_{k+1}(j)] \quad (\text{III.25})$$

Note again that each filter will operate with a distinct value of the motor torque/back-emf constant. Thus, two fault cases exist. First, the actual faulted value could be identically equal to that used in one filter model. Or, secondly, the faulted value could be located between the values used for two of the filters. The net generalization is that only two filters ever need to be considered.

We choose the two filters for consideration based on the computed errors. Of the N filters, filters α and β are chosen as the two with the smallest errors. A total error is defined as indicated in (III.26).

$$E_{\text{tot}} = E(\alpha) + E(\beta) \quad (\text{III.26})$$

A weighting factor, W , for each filter, α and β , is computed as shown in (III.27) and (III.28).

$$W(\alpha) = 1 - \frac{E(\alpha)}{E_{\text{tot}}} \quad (\text{III.27})$$

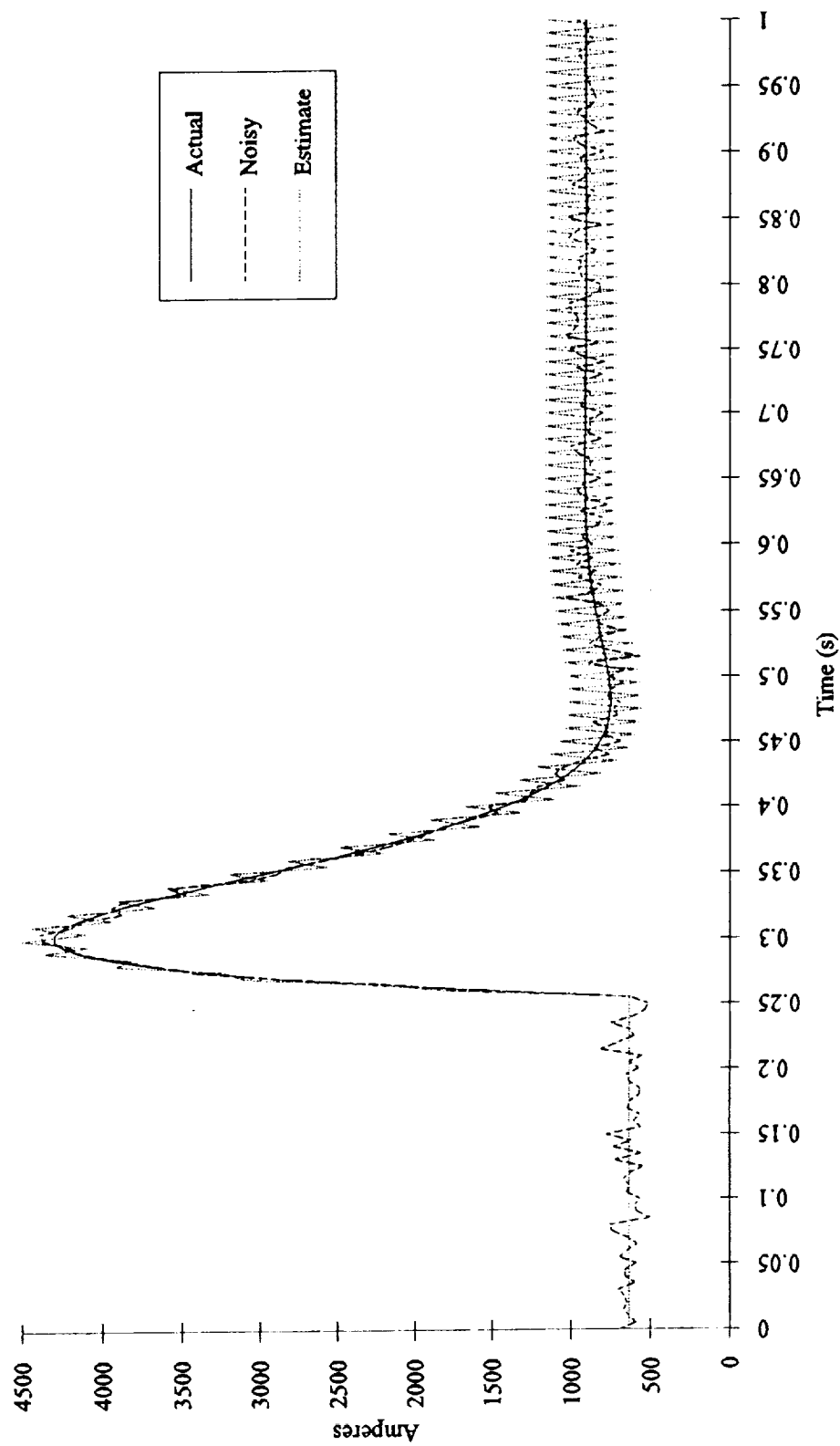
$$W(\beta) = 1 - \frac{E(\beta)}{E_{\text{tot}}} \quad (\text{III.28})$$

The final estimated state at time k is computed as presented in (III.29).

$$\hat{\mathbf{x}}_k = W(\alpha)\hat{\mathbf{x}}_k(\alpha) + W(\beta)\hat{\mathbf{x}}_k(\beta) \quad (\text{III.29})$$

The previously presented motor was again used for example. At 0.25 s, the motor torque/back-emf constant was reduced to 70% of the nominal value. A bank of five filters using k_m values of 20, 40, 60, 80, and 100% of the nominal value were employed. The simulation began under steady-state conditions. All injected noise was zero mean. The current and speed noise standard deviations were 75A and 5 rad/s, respectively. Figures III.6 and III.7 show the results for armature current and rotor speed, respectively. It should be noted that if either the α or β weighting factors were greater than 0.8, the corresponding filter estimate was used solely rather than in combination with the other chosen filter.

Figure III.6. Armature Current.



While the estimate does track the general trend, oscillation in the current estimate is clearly visible. If the only requirement of the monitoring system is to indicate the presence of a disturbance, then the objective is fulfilled. However, if we wish to produce reliable estimates and accurate fault representations, then we must produce a more reliable estimate.

Note that the oscillation on the current estimate is produced by repeated switching between two filters. Specifically the filters with k_m at 60 and 80% of the nominal value (Recall that the actual value was 70% nominal.). This type of "chatter" is quite easily characterized. The highest frequency of the chatter will occur when the most likely filter changes every estimation cycle. Thus, the period of oscillation will be twice the estimation time step. Note that this is the highest frequency component available for waveform reconstruction as dictated by the Nyquist sampling rate.

Low pass digital filtering techniques allow a substantial reduction in the chatter. For illustration, a discrete time model of the simplistic low pass filter illustrated in Figure III.8 was employed as a digital filter.

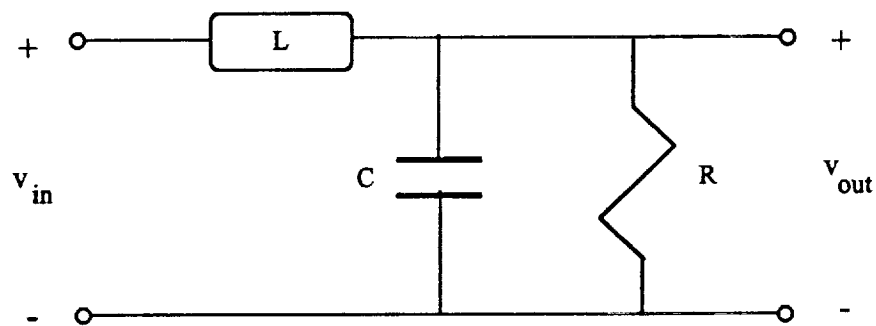
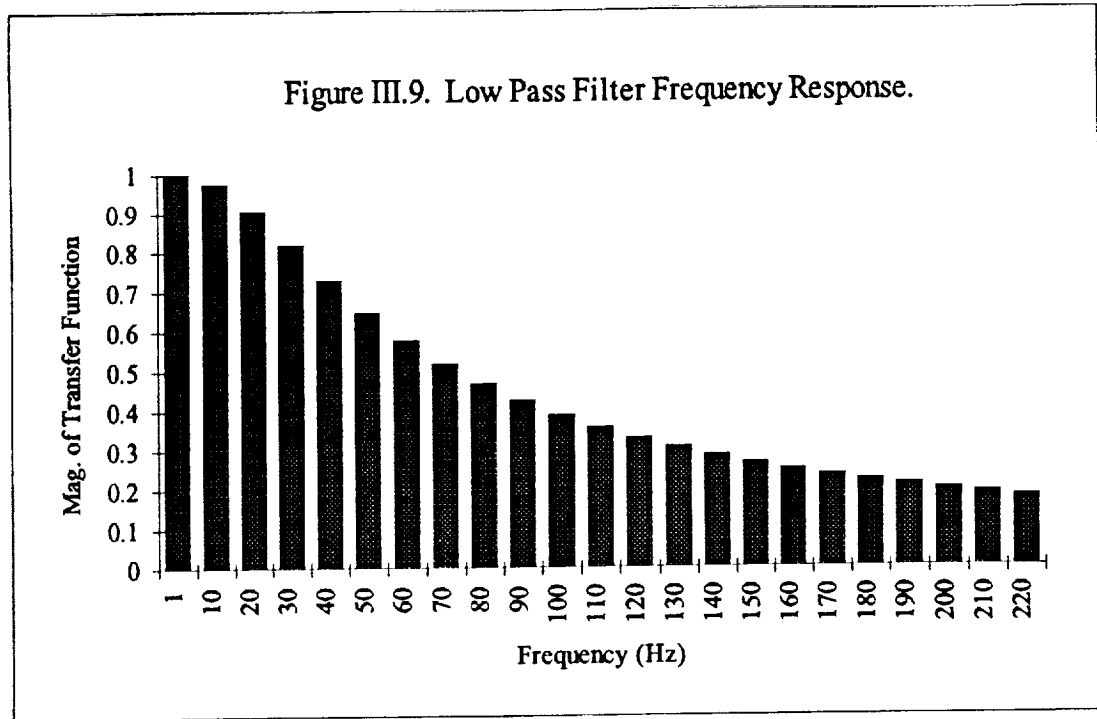


Figure III.8. Simple Low Pass Filter.

The filter component values were chosen for the frequency response as illustrated in Figure III.9. Note that this figure shows the magnitude of the transfer function versus frequency.

Figure III.9. Low Pass Filter Frequency Response.



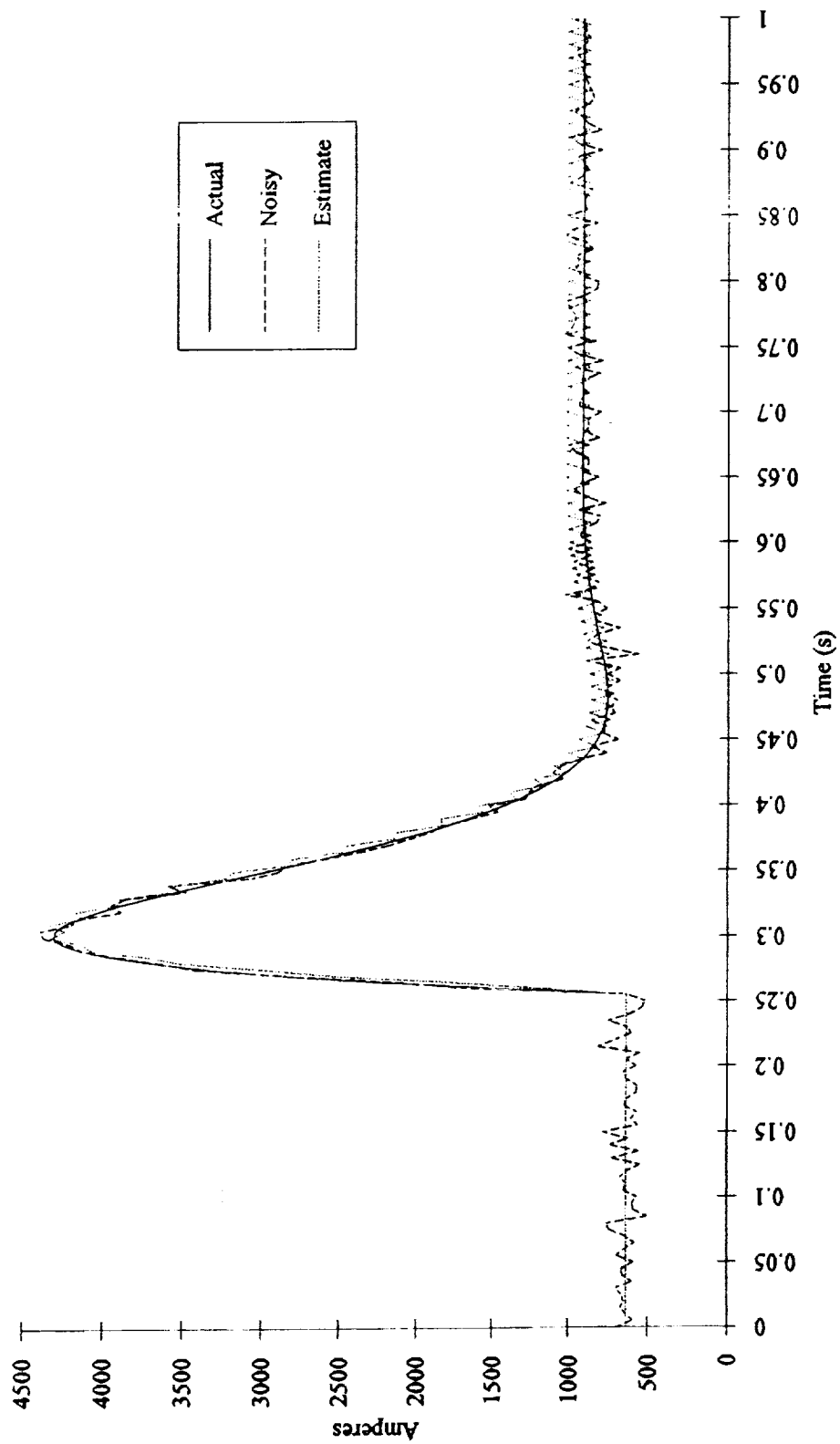
This filter is certainly not optimal. However, it does provide information as to the feasibility of filtering the estimate. Figure III.10 shows the estimation results for the armature current in the previous example after application of the low pass filter. The results are quite promising.

Extraction of the system parameters warrants discussion. As the system state is estimated at each point in time, the torque constant can be estimated. In fact, the estimate can be performed with the same weighting factors used in the armature current calculations. This is shown in (III.30), where the "hat" notation indicates an estimate.

$$\hat{k}_m = W(\alpha)k_\alpha + W(\beta)k_\beta \quad (III.30)$$

Above, k_α and k_β represent the values of k_m assigned to filters α and β , respectively. However, this estimate, as one would expect, displays the same chatter as seen in the current estimate. A digital low pass filter identical to the one designed for current

Figure III.10. Filtered Armature Current.



filtration can be applied to this signal as well. Figure III.11 shows the estimated and filtered results for the motor torque constant. Note that the actual values are also displayed.

The Kalman/low pass filtering algorithm has been extensively tested to date for the single fault presented herein. Specific details about continuing efforts will be presented in the next section. We will state here, however, that modifications and optimization is being performed in the low pass filter stage of the estimator.

III.4. Continuing Efforts

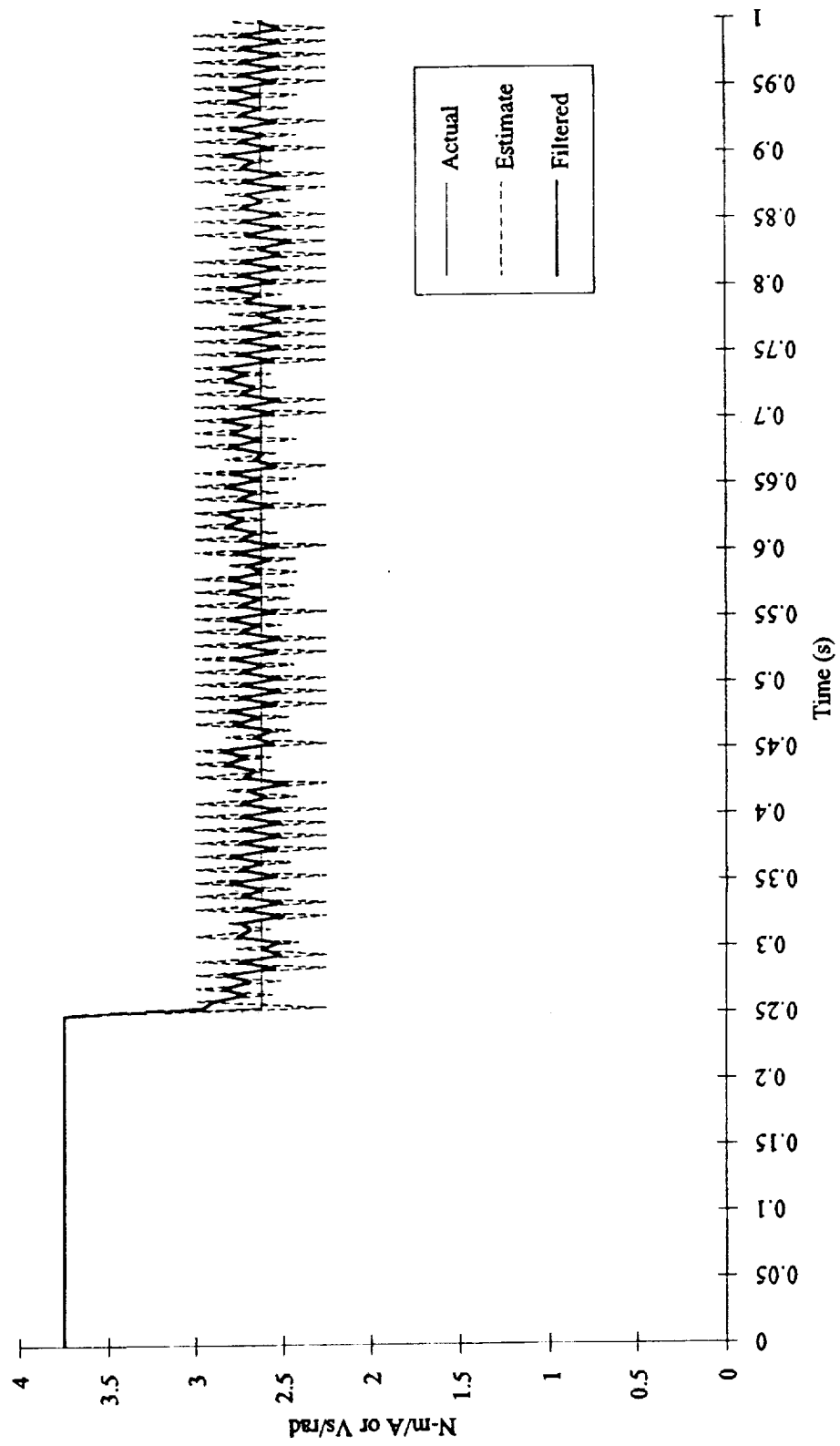
At this stage of our work, we are extending and verifying the efforts that have been reported. The low pass filter is being optimized, and other estimate filtering strategies are being investigated. For example, notch filtering is being considered to reduce chatter even further than possible with strictly low pass filtering, but yet leave sufficient frequency content to accurately track large signal swings.

In addition to filter optimization for the adaptive architecture, the linearized Kalman filter is still under consideration. Efforts are ongoing to use an iterative approach with minimal computational overhead. However, we feel that when a final decision as to estimator architecture is reached, it will be the adaptive structure.

The adaptive structure for the Kalman filter is being extended to handle changes in other system parameters such that all pertinent faults can be detected. Rather than a one dimensional bank of filters, the bank will consist of multiple dimensions. One dimension will be created for each parameter of interest. This scheme promises to be extremely effective, cost efficient, and of minimal size and complexity.

We are comparing the application of modular health monitoring and fault diagnosis systems (one system for each major component with a supervisory processor) with an overall system estimator as one unit. Currently, an estimator for an entire BDCM and

Figure III.11. Motor Torque/Back-emf Constant.



PWM drive system is under design. However, we presently feel that widely separated time constants associated with the various actuator components will push us toward selecting the modular approach.

III.5. Hardware Implementation

To provide a realistic assessment of the feasibility of use of the described health monitoring and fault diagnosis strategy, we are planning to construct an integrated circuit based implementation of the small system previously presented. Toward this end, the assistance of Dr. Larry Wurtz, of The University of Alabama Electrical Engineering Department, has been enlisted. Currently we are in the process of converting the optimized software version of the filter into digital logic designs. The device will constitute a special purpose processor. With a completed design at the chip level, fabrication will begin.

Hardware verification and testing will be performed in The University of Alabama Electrical Engineering Department's Power/Machines Laboratory. This facility houses the configurable machine apparatus described in the last progress report. We expect that this effort will produce substantial transfer of technology through journal publication.

III.6. References

- [III.1] Weerasooriya, Siri and M.A. El-Sharkawi, "Adaptive Tracking Control for High Performance DC Drives," IEEE Transactions on Energy Conversion, Vol. 4, No. 3, pp. 502-508, September 1989.
- [III.2] El-Sharkawi, M.A. and Siri Weerasooriya, "Development and Implementation of Self-Tuning Tracking Controller for DC Motors," IEEE Transactions on Energy Conversion, Vol. 5, No. 1, pp. 122-128, March 1990.

- [III.3] El-Samahy, A.A., et. al., "Adaptive Multi-Layer Self-Tuning High Performance Tracking Control for DC Brushless Motor," IEEE Power Engineering Society Paper No. 93 SM 456-4 EC, 1993.
- [III.4] Brown, Robert Grover and Patrick Y.C. Hwang, Introduction to Random Signals and Applied Kalman Filtering, Second Edition, John Wiley and Sons, Inc., 1992.
- [III.5] Haskew, Tim A. and David Jeff Jackson, "Real-Time Simulation of a Six Pulse Inverter," Proceedings of the Twenty-Third Annual Pittsburgh Modeling and Simulation Conference, Vol. 23, Part 4, pp. 2049-2056, 1992.
- [III.6] Krause, Paul C., Analysis of Electric Machinery, McGraw-Hill, Inc., 1986.
- [III.7] Zai, Li-Cheng, et. al., "An Extended Kalman Filter Approach to Rotor Time Constant Measurement in PWM Induction Motor Drives," IEEE Transactions on Industry Applications, Vol. 28, No. 1, pp. 96-104, January/February 1992.

A Research Grant Proposal
TO BUILD A ROLLER SCREW TEST STAND

SUBMITTED TO:

NASA
Marshall Space Flight Center AP16
ATTN: Ray Miller

PREPARED BY:


Dr. Timothy A. Haskew Assistant Professor Department of Electrical Engineering	Dr. John Wander Assistant Professor Department of Mechanical Engineering
--	--

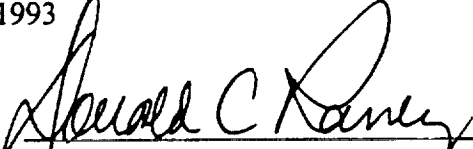
College of Engineering
The University of Alabama
Box 870276
Tuscaloosa, AL 35487-0276
and
The Bureau of Engineering Research
College of Engineering
The University of Alabama
Box 870201
Tuscaloosa, AL 35487-0201

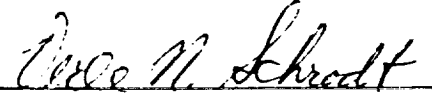
SUBMITTED BY:

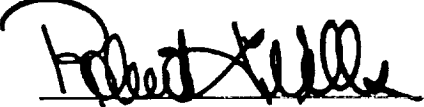
The University of Alabama
Box 870104
Tuscaloosa, AL 35487-0104

BER Proposal No. 3544
August 1993


John Wander
Project Director


Donald C. Raney, Head
Department of Mechanical Engineering


Verle N. Schrod, Assistant Dean
for Research and Graduate Studies


Robert L. Wells, Assistant Vice-
President for Research

APPENDIX A

Test Stand Constuction Proposal

TABLE OF CONTENTS

1 Introduction	1
2 Design of the Test Stand	1
2.1 Computer Control and Data Acquisition System	2
2.2 Instrumentation	2
2.3 Bearing Frame	3
2.4 Actuators	6
3 Experiments	7
3.1 Transient Loading Experiments	7
3.2 Transverse Loading Experiment	7
3.3 Friction Experiment	8
3.4 Flexibility for Future Experiments	9
4 Summary	9
Appendix A: Proposed Budget	10
Appendix B: Parts Lists	11

1 Introduction

A general-purpose test stand has been designed in association with NASA Grant NAG8 240 to study electromechanical actuators for space application. The stand is designed to allow a variety of test and verification experiments for both TVC and other space applications. The stand can be used with a roller screw in isolation or with an entire TVC or other actuator. The immediate goal of the test stand is to determine the effects of the startup transients and transverse loads that can be expected in TVC applications with the SME and to assess various alternative actuator designs in terms of overall efficiency, reliability, and fault detection. We propose to build the test stand at The University of Alabama for \$22,716. Once built, the stand will be used in accordance with ongoing research under NASA Grant NAG8 240.

2 Design of the Test Stand

The test stand under development is meant to allow experiments with both the electrical actuation and screw transmission of the developing class of EMAs designed for space application. Since questions about reliability, fault detection, fault tolerance, and modeling for control synthesis exist, the potential applications of the stand are very broad. This fact directs one toward a versatile design. At the same time, specific questions about transient shock loading and transverse loading of the TVC actuator for the SME require some specific capabilities. The following represents the basic design objectives that were set:

- to study transient loading of up to 100,000 lbf at 6 Hz
- to study transverse loading of 1000 lbf at 6 in/s travel against 30,000 lbf load
- to provide multiple coupling options between actuators and screws
- to allow mounting of an entire SME TVC actuator
- to provide for placement in a controlled environment

2.1 Computer Control and Data Acquisition System

A variety of control and data acquisition system possibilities were considered with cost and system adaptability of prime importance. The hardware cost for the suggested system is \$3000. The computer requirements for the various tests to be performed differ widely. Simple static compliance tests could be performed without computer control while experimentation with active compliance with shock loading requires both high-speed control and data acquisition. With this variety of requirements and the possibility of additional requirements associated with still undefined experiments, it was decided to use a PC buss for which the widest variety of peripherals are inexpensively available. The system selected was a compromise between desired experimental capabilities and hardware costs. Detailed specifications and costs are listed in Table B1 of Appendix B. The general specifications met by the system are:

- 20 channels of differential A/D (25 kHz sampling on each of 4 channels)
- simultaneous sampling on at least 4 channels, preferably 8
- 4 channels of simultaneous analog output
- 3 channels of digital parallel I/O
- selectable system sampling period

2.2 Instrumentation

The instruments thus far specified are designed to measure loads and displacements. Other quantities important to the investigation of mechanical TVC performance are bearing surface quality and possibly coating thicknesses and roller roundness. Measurements of these quantities will not be made on-line and it is anticipated that instruments will be available without special purchase. Currents can be measured in a variety of ways with inexpensive transducers and the specified analog to digital capabilities of the data acquisition system. Instruments that have been specified thus far are listed in Table B2 in

Appendix B along with required supporting electronics. The total cost is \$8600 though over \$3700 can be saved by not equipping to develop detailed friction models.

2.3 Bearing Frame

First and foremost, the stand had to bear the 100,000 lbf shock loading used to simulate engine startup transients. In order to simplify the design procedure and incorporate a factor of safety, the 100,000 lbf transient loading was considered to be a static load of 200,000 lbf. Support of this load requires large structural members.

Since large structural members were required, it was considered best if the stand was a frame like structure constructed in the horizontal plane. Figure 1 shows the preliminary design of the test stand. A test bed width of 36 inches would provide enough room for easy access to all the different components, while not being so large as to cause space allocation problems. The test bed internal span length was designed to be variable from a maximum of 72 inches to a minimum of 24 inches. This provides for much flexibility in the types of roller screws that can be tested.

With the preliminary size constraints known, the calculations for the proper size structural members could be made. The resulting structure is statically indeterminate and required the use of Castigliano's theorem for analysis. The suggested structural members are W12x87's, which provide adequate strength to protect against failure at all critical points.

Once the proper frame members were selected, the connections had to be designed. An eight tension bolt end-plate connection was chosen for its strength and simplicity. This design resulted in the use of a 3/4 inch thick end plate in conjunction with twelve one inch diameter A325-N bolts and one 3/4 inch thick stiffener. The end plates are welded to the ends of the cross members which are then bolted to the longitudinal members. This design allows the test fixture to have a variable test bed length since it is bolted together and not welded.

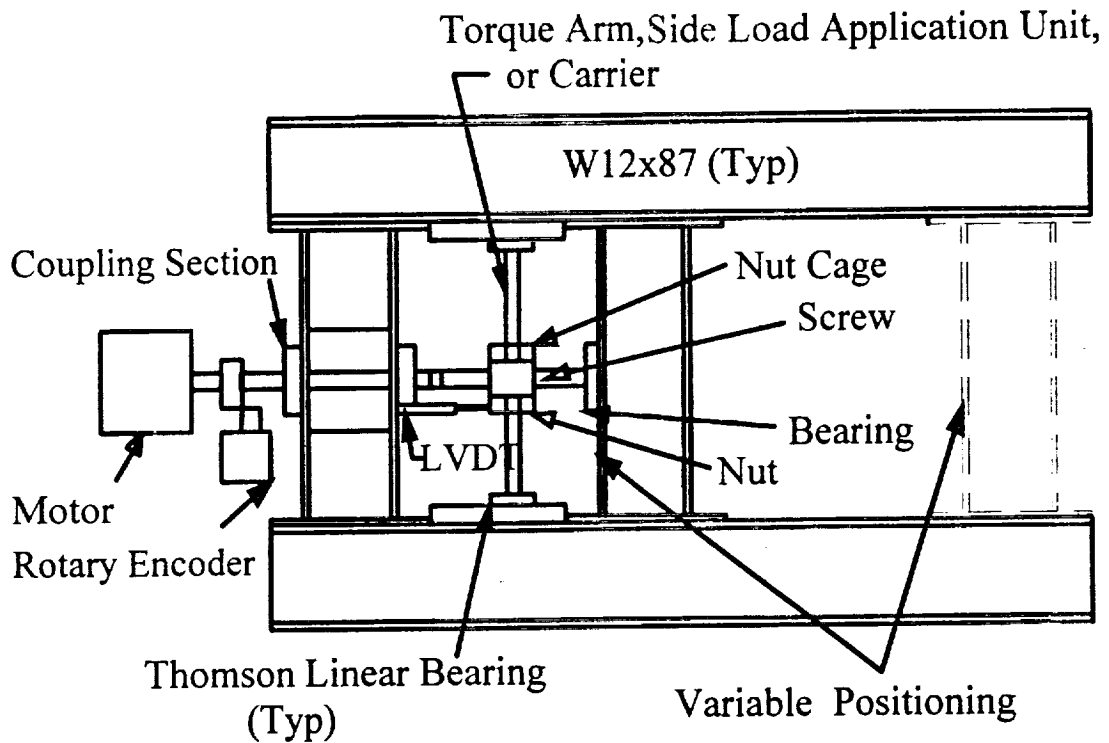


Figure 1 Scale Drawing of Roller Screw Test Stand

With the basic frame in place, the next step was to design a coupling system that would withstand the required loading and be flexible enough so as to accommodate different motors and screws. Since different tests would require different loading conditions, it was necessary to have a system that was capable of bearing both axial and radial loads. This was accomplished by using both a spherical roller bearing and a tapered roller bearing. This combination, shown in Figure 2, is capable of handling high loads for short periods of time and moderate loads for a long periods of time. The advantages of this system can easily be seen from the figure. The locations of the bearings make access to them relatively easy, while the integration of the structural member into the assembly allows for a very high load bearing capability.

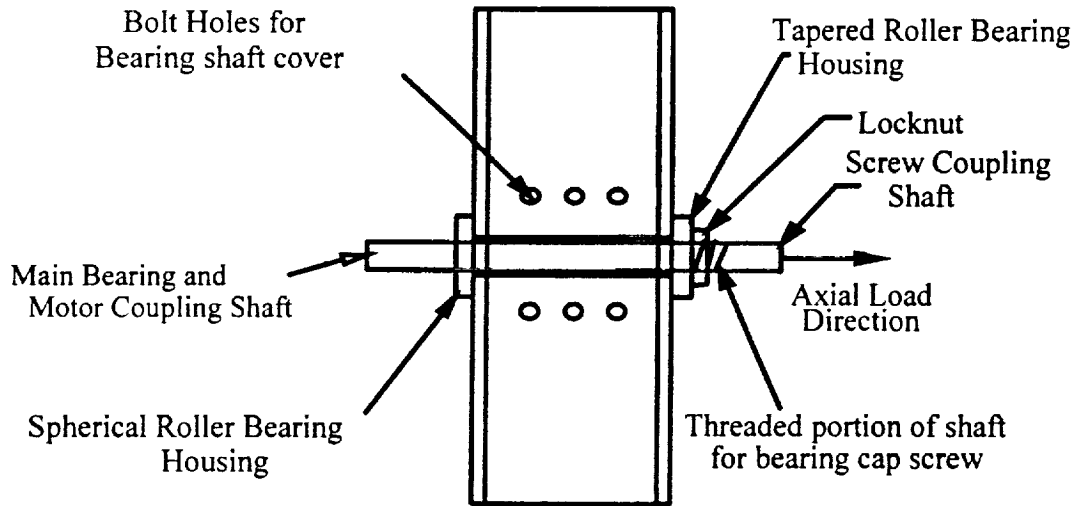


Figure 2. Coupling System

As previously mentioned this system requires two bearings for a proper working configuration. This is due to the fact that the spherical roller bearing requires a minimum load of 20 lbf. This minimum load can be achieved by placing a tapered roller bearing on the opposite flange of the structural member and using a threaded locknut to hold the bearing in place. In this way the shaft at the point of the tapered roller bearing can be threaded and the locknut can be tightened down until the desired minimum load is achieved. This extra bearing also provides for added stability for the coupling shaft.

A linear bearing system was designed to support the screw while allowing measurement of relevant loads and displacements. For thrust vector control, the nut rides in a carrier while one end of the screw is unsupported. One way to achieve this configuration is to use two linear bearing systems that act as carriers for the nut. In this way the two systems restrict the nut's rotation while allowing it to travel in the axial direction, thus closely approximating the actuator for thrust vector control. This system is shown in Figure 3.

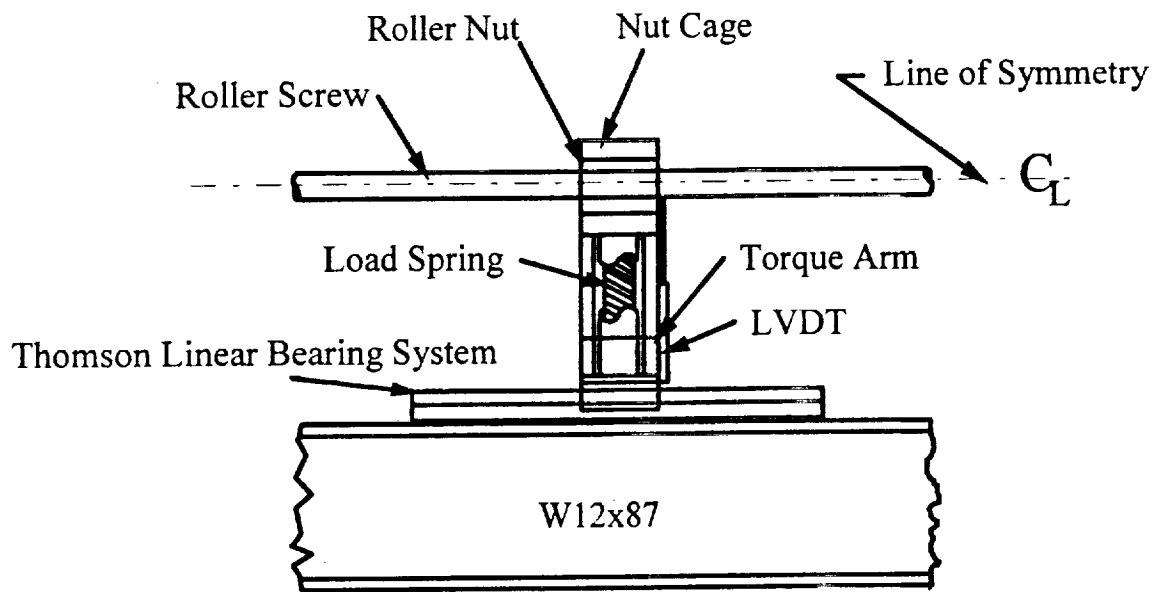


Figure 3. Linear Bearing System

These linear bearings can have many different functions depending upon the type of experiment being conducted. They can serve as the platform for applying side loads during the transverse loading experiments. They can also be used as a platform for measuring large torques produced by the nut. This can be accomplished by using the carrier arm in conjunction with a load cell as a dynamometer. In addition to the aforementioned uses, the linear bearing system could also be used to carry a LVDT that would measure transverse deflections. The total cost of the structure if it is built at UA is estimated to be \$3900 allowing \$1500 for machining and assembly.

2.4 Actuators

One option for loading the roller screw is to use hydraulics. The use of hydraulics allows many different types of tests to be performed at reasonable costs. Planned experiments include transient loading of 100,000 lbf, driving the nut against a 30,000 lbf load at 7 in per sec, and a passive damping test where the nut is driven at 6 Hz. The hydraulic equipment required to perform the tests costs approximately \$4,125. The required equipment is listed in

Table B4. The components in this list are only suggested parts and substitution of equivalent components is easily accommodated. Also, if NASA should have any of this equipment available for long term loan, the cost of the system could be greatly reduced.

The 8" bore cylinder would be capable of providing the 100,000 lbf load for the transient loading tests, while the 4 1/4" bore cylinder would be used to drive the nut against various loads up to 30,000 lbf at 7 in/sec. Also, the 2 1/4" bore cylinder would be used in conjunction with the 6 Hz servo valve to drive the nut at 6 Hz with a peak to peak amplitude of 1.3 inches. The same basic hydraulic system would be used with each cylinder, and the cylinders would be interchanged as required for each test. Details of mounting the hydraulics have yet to be determined.

In addition to the axial load application, a motor is required for driving the roller screw. A servo drive and motor can be obtained for approximately \$2500 that will be adequate for initial experiments. Again, it is possible that NASA Marshall will have a motor and drive available that could be loaned temporarily to UA.

3 Experiments

3.1 Transient Loading Experiments

Axial loads of various frequencies and magnitudes must be applied to study the effects of startup transient loads on the bearing system and to determine the ability of the actuator to be backdriven. In order for these experiments to be conducted, a system for loading the actuator will have to be developed. Also, these loads will need to be measured. This will require placing rod-in-line threaded load cells at the point of load application.

3.2 Transverse Loading Experiment

This particular experiment requires that side loading be applied to the actuator. The side load will be applied using a spring loaded system that will be carried by one of the linear bearings. This system is represented, except for minor differences, in Figure 3 above. The

difference between the figure and the actual system is that there is only one linear bearing system used. As the previous statement implies, this means that the nut will not be carried by the linear bearings, instead the roller screw will be supported by an additional tapered roller bearing located at the variable end of the test bed.

The spring loaded system will include a spring with a stiffness of 1650 lbf/in placed in a 2 inch diameter SCH 40 pipe. The spring will be compressed by a threaded rod and plate arrangement, and will apply the load to the nut through a 1 1/2 inch diameter pipe that will slide inside the 2 inch diameter pipe. A load cell will be placed between the 1 inch diameter pipe and the nut cage. This will allow the magnitude of the side load to be accurately measured.

Other requirements of this test include measuring the transverse deflections of the screw and the torque seen by the nut. The transverse deflections of the screw will be obtained by simply mounting a LVDT on the linear bearing perpendicular to the screw. Also, if large enough, the torque seen by the nut will be measured by using a torque arm and load cell combination in a dynamometer configuration (see Figure 3). This will be accomplished by attaching angles to the linear bearings and placing load cells at the point of contact of the torque arms. However, if the resultant torques are too small to be practically measured by the torque arm, an in-line torque sensor will be used.

3.3 Friction Experiment

For the friction experiments, the key factors are the measurement of rotary and axial displacements, and torque. For the rotary displacement measurements, it will be necessary to use a rotary encoder geared from the main shaft. For the axial displacement measurement, a LVDT will be mounted as shown in Figure 1. Also, for the torque measurements, an in-line torque sensor will be used since the associated torque will be small.

3.4 Flexibility for Future Experiments

Not all experiments can be envisioned at this time, however, the features of this test fixture were designed to provide the maximum flexibility for future use. Such features include bolted components and connections, space for additional components, allowance for variable positioning of the test bed, and a multipurpose coupling system that allows for the use of many different types of motors and actuators.

4 Summary

The test stand described above provides for experiments with transient loading, transverse loading, friction modeling and fault detection. It has been designed to allow a wide variety of additional experiments with only minor alterations or additions. For example, the stand allows for the placement of an entire actuator in the test bed and being placed in controlled a environment. The ability to test in vacuum will be useful to study performance of actuators for deep space missions.

A breakdown of the required individual parts and their associated costs is given in Tables B1 through B4 Appendix B. Some of the parts listed in the tables are still tentative choices, however, they provide a good estimate part cost that totals \$20,592. Including a \$1500 allowance for fabrication and the associated \$624 of indirect costs, the total cost for construction of the test stand at The University of Alabama is \$22,716.

Appendix A: Proposed Budget

Period of Performance: 9/16/93 - 8/15/94

A.	Fabrication Services	\$1,500
B.	Equipment Roller Screw Test Stand (to be constructed)	\$20,592
	Total Direct Costs	\$22,092
D.	Indirect Costs @ 41.6% MTDC	\$624
	Total Costs	\$22,716

APPENDIX B

Detailed Test Stand Drawings
(Not to Scale)

Appendix B: Parts Lists

Table B1 Computer and Data Acquisition Hardware

Item	Model	Qty.	\$/Unit	\$
PC		1	\$150000	\$1500.00
I/O	CIO-DAS/16/330 (Computer Boards Inc..)	1	\$799.00	\$799.00
	CIO-SSH16 simultaneous sample & hold	1	\$399.00	\$399.00
	CIO-SSH-AMP	1	\$ 39.00	\$ 39.00
	C37FF cables	2	\$ 25.00	\$ 50.00
	C37FFS cables	6	\$ 30.00	\$ 180.00
	CIO-MINITERM	1	\$ 49.00	\$ 49.00

Table B2 Instrumentation

Item	Model	Qty.	\$/Unit	\$
TorqueArm Load Cell	(Sensotec)AL112DR	2	\$485	\$970
	BE 123	2	\$245	\$490
Thrust Load Cell	(Sensotec)AL417EP	2	\$690	\$1380
	2a	2	\$135	\$270
Side Load Cell		1	\$135	\$135
	2a	1	\$135	\$135
In-Line Torque Sensor	(SHC)2801T(25-0)	1	\$3035	\$3035
	61201DL	1	\$755	\$755
LVDT (Transverse)	BY132HR(Sensotec)	1	\$475	\$475
LVDT (Axial)	DCTM-36(Temposonics)	1	\$806	\$806
Rotary Encoder	73(Leine&Linde)	1	\$100	\$100

Table B3 Structural Parts and Bearings

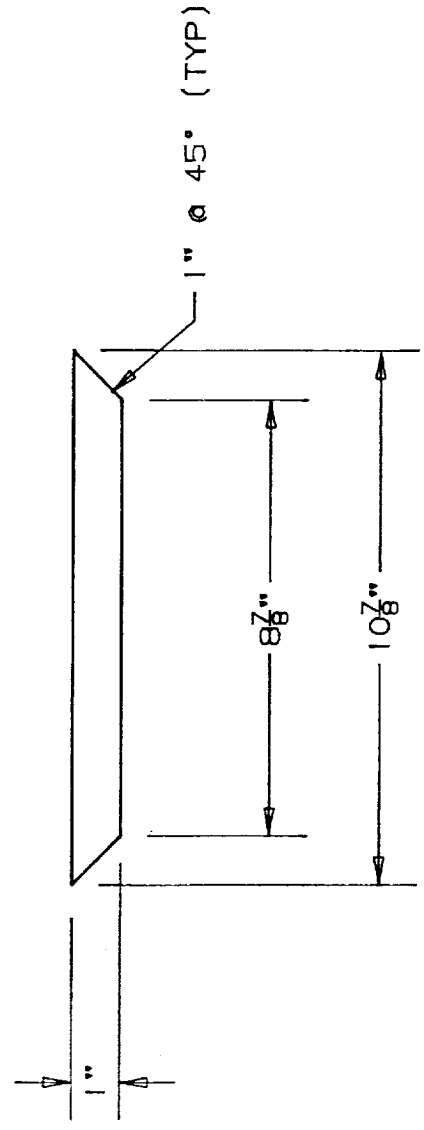
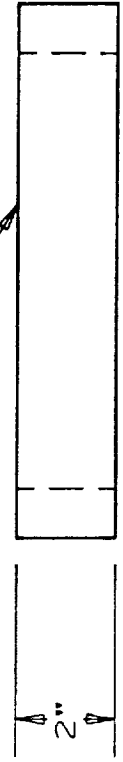
Item Description	Part Number	Qty.	\$/Unit	\$
Structural Plates				\$80
Structural I Beam	W12x87	50Ft.	\$12/Ft.	\$600
Spherical Roller Bearing	(SKF)29412E	1	\$380	\$380
Tapered Roller Bearing	(Timken)476,472	2	\$50	\$100
Thomson Linear Bearing	1CC-16-HAAL18	2	\$620	\$1240

Table B4. Actuators

Description	Model	Qty	\$
40 Hp Electric Motor	GE 5K286JD120	1	\$1250
26 GPM, 2500 psi Gear Pump	JSB 4F675	1	\$225
6Hz, 26 GPM, 2500 psi Servovalve	Moog 631	1	\$1200
8" Bore x 2" Strk. x 2" dia. Rod	DTE	1	\$350
4 1/4" Bore x 12" Strk. x 2" dia. Rod	DTE	1	\$350
2 1/4" Bore x 4" Strk. x 3/4" dia Rod	DTE	1	\$250
40 HP servo motor and drive			\$2500
Other Miscellaneous Parts	N/A	-	\$500

MATERIAL	DESCRIPTION
	PL. 1" X 2" X 10-7/8"

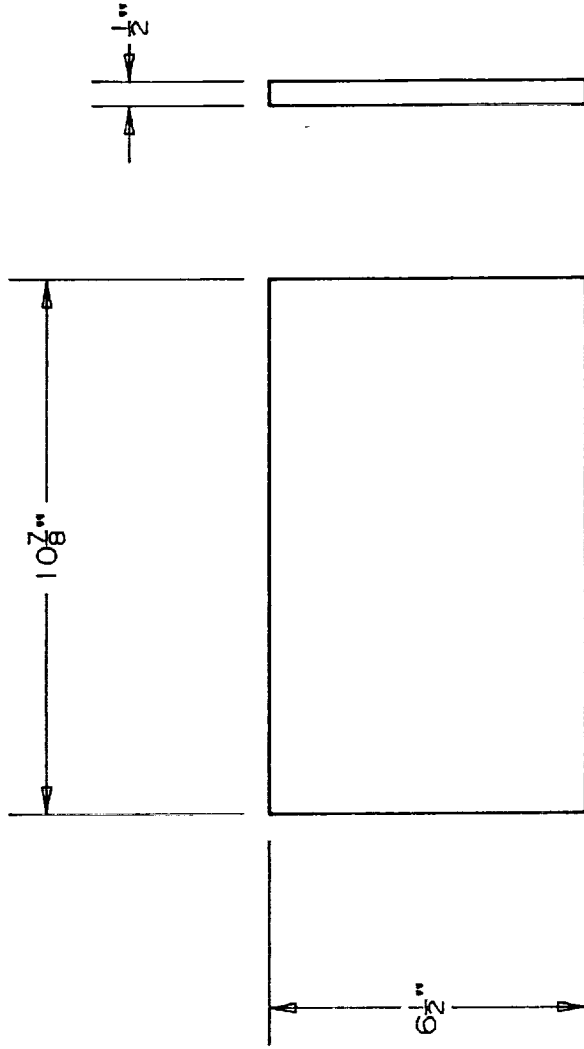
7



REFERENCE	
TEST STAND	
SCAB PLATE	
DATE	DRAWING NUMBER
10	10

REV.	BY	DESCRIPTION	DATE

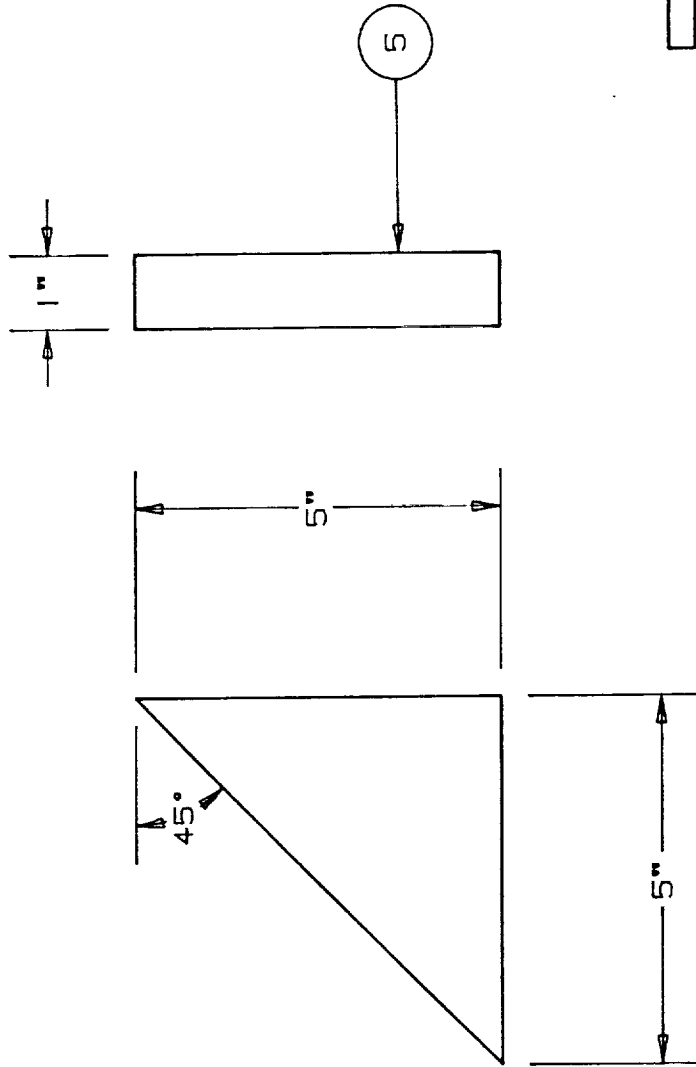
MATERIAL	DESCRIPTION
	PL. 1/2" X 6-1/2" X 10-7/8"



REFERENCE	
TEST STAND	
COVER PLATE	
DR. SEP	
DATE	
WORKS	
DATE	10-7-79
REV	9

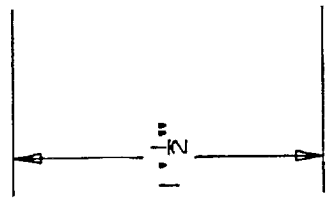
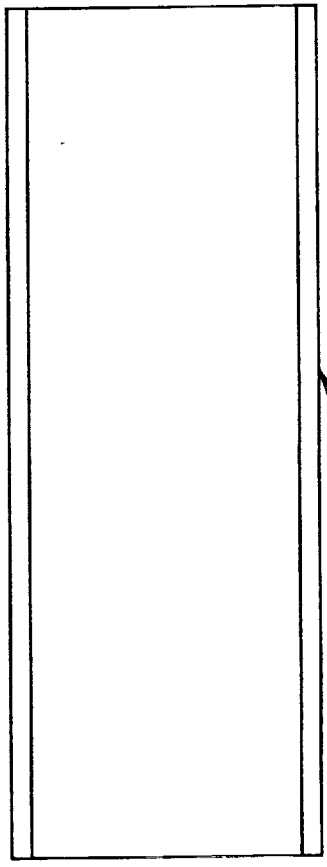
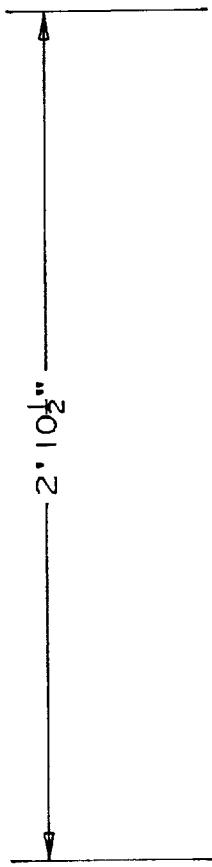
REV.	BY	DESCRIPTION	DATE

MATERIAL	DESCRIPTION
	PL. 1" X 5" X 5"



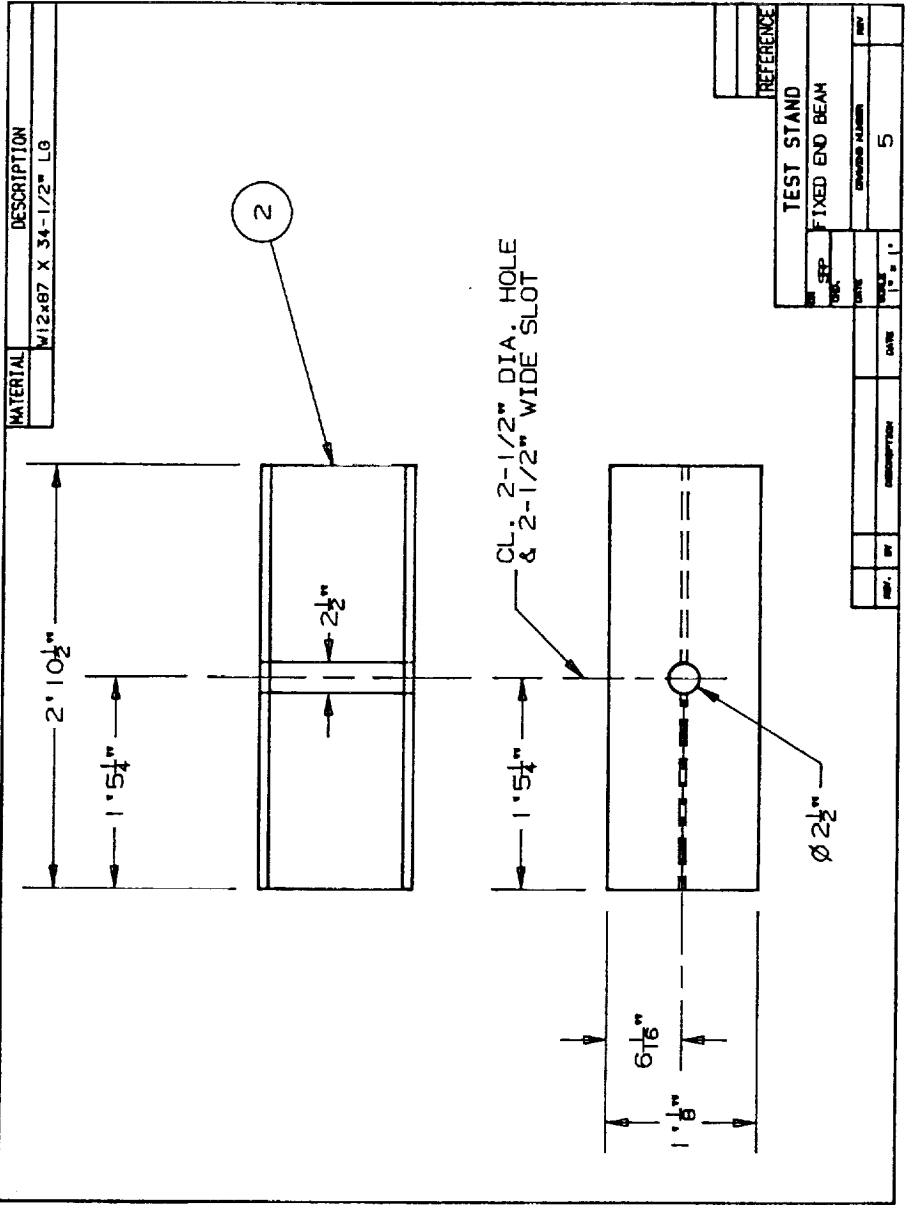
REV.		BY	DATE	DESCRIPTION
DATE		NOCK	DATE	
GUSSET		NOCK	DATE	
TEST STAND		NOCK	DATE	
DRAWING NUMBER		NOCK	DATE	
8		NOCK	DATE	

MATERIAL	DESCRIPTION
	W12x87 X 34'-1/2" L.G.

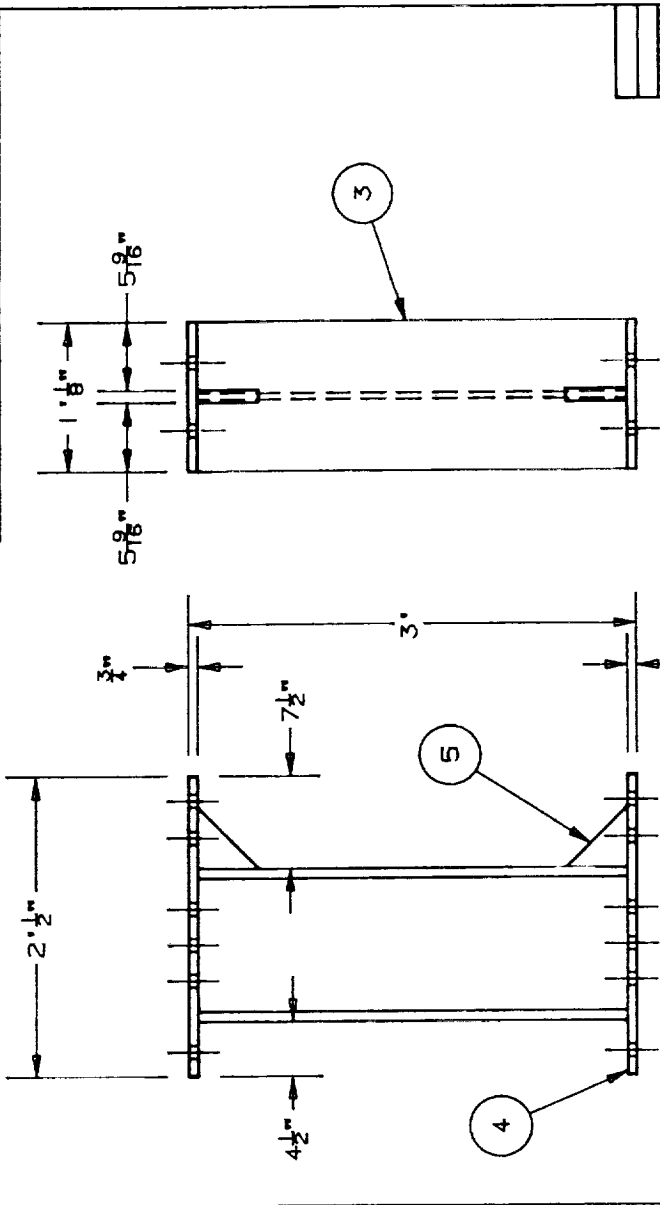


3

REV.	BY	DESCRIPTION	DATE
TEST STAND			
IN. SEP.	DATE	WORK	SCALE
ADJUSTABLE END BEAM		2" = 1'	
REV.	DATE	DRAWING NUMBER	REV.
		6	



PC. #	QTY	REQD.	DESCRIPTION
3	6	1	ADJUSTABLE BEAM
4	7	2	END PLATE
5	6	2	BUSSET

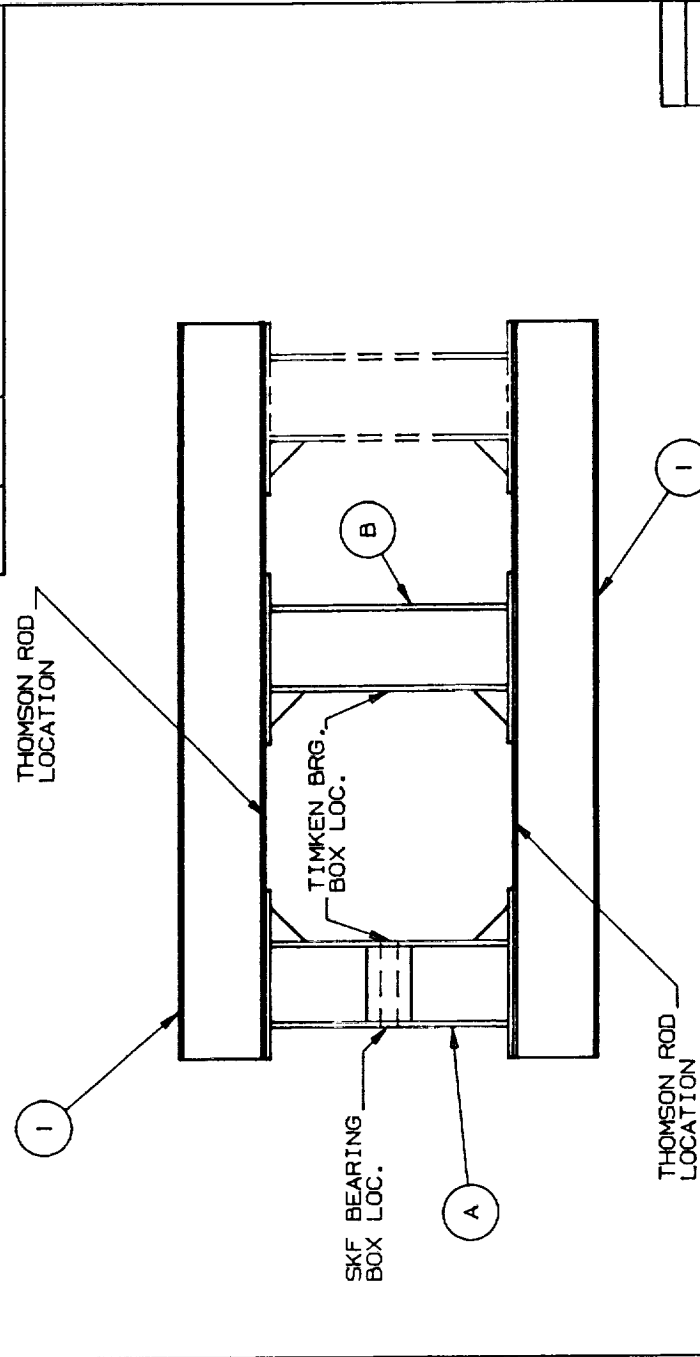


NOTE: END PL & STIFFENER TO BEAM WELD = 3/8" FILLET

REFERENCE	
TEST STAND	
ASSEMBLY 'B'	
CHANGED NUMBER	4

REV.	BY	DATE	DESCRIPTION

PC. #	DWG. #	DESCRIPTION
1	2	SIDE BEAM
A	3	ASSEMBLY 'A'
B	4	ASSEMBLY 'B'



REFERENCE	
TEST STAND	
PLAN VIEW OF TEST STAND	
DRAWING NUMBER	1

REV.	BY	DESCRIPTION	DATE
			5/08 = 11